Experiments on vertical and streamwise dispersion of tracer stones under lower-regime plane-bed equilibrium bedload transport

Miguel Wong[1], Gary Parker[2], Paul DeVries[3], Timothy M. Brown[4] and Stephen J. Burges[4]

[1]: Barr Engineering Company, Minneapolis, MN, USA

[2]: Ven Te Chow Hydrosystems Laboratory, Departments of Civil and Environmental Engineering and Geology, University of Illinois, Urbana, IL, USA

[3]: R2 Resource Consultants, Redmond, WA, USA

[4]: Department of Civil and Environmental Engineering, University of Washington, Seattle, WA, USA

Abstract

A common approach for estimating the bedload transport rate in gravel-bed streams is to relate it to deterministic channel-averaged driving parameters and corresponding resistance properties of the bed material. Notwithstanding the proven success of this approach in modeling various morphodynamic scenarios, it does not contain the mechanics necessary to relate the bulk sediment transport rate to the displacement patterns of individual particles. Experiments on entrainment, transport and deposition of tracer stones in a flume described here were designed to address this issue. Predictors of statistics of bed elevation fluctuations at short time scales, total and elevation-specific particle entrainment rates, particle step lengths, mean and associated probability density function for particle virtual velocity, and thickness of the active layer were developed. The working hypothesis tested in this paper is that the statistics of tracer displacements can be related to channel-averaged hydraulic parameters, and thus linked to macroscopic aspects of bedload transport. *INDEX TERMS:* 1625 Geomorphology - Fluvial; 1815 Hydrology - Erosion; 1861 Hydrology - Sedimentation; 1862 Hydrology - Sediment transport; *KEYWORDS:* bedload transport, gravel-bed streams, tracer stones, active layer, particle virtual velocity, particle entrainment.

1. Introduction

Mountain streams transport large amounts of coarse bed sediment, including sand, gravel and in some cases cobbles and boulders. Coarse material moves primarily in the form of bedload, with particles sliding, rolling or saltating within a thin layer near the streambed. Transport events of significance are typically associated with floods [*Kuhnle*, 1992; *Schmidt and Ergenzinger*, 1992; *Gintz et al.*, 1996; *Ferguson and Wathen*, 1998; *Haschenburger and Church*, 1998; *Lenzi*, 2004]. Bedload particles move sporadically during these events [*Schick et al.*, 1987a, 1987b; *Tsujimoto et al.*, 1990; *Niño et al.*, 1994; *Malmaeus and Hassan*, 2002; *McEwan et al.*, 2004], either under conditions of partial or full mobility [*Wilcock*, 1997a; *Hassan and Church*, 2000; *Wu and Yang*, 2004]. Knowledge of the displacement patterns of individual particles can help to improve prediction of the overall morphodynamic response of a stream to water discharge and sediment supply conditions. Such an understanding is the main goal of the work presented here.

Modeling the morphodynamic evolution of a bedload-dominated stream requires solving the continuity and momentum equations for both water and sediment. With regard to sediment, this can involve a range of approaches, from more complex discrete particle modeling [see e.g., *Schmeeckle and Nelson*, 2003; *Heald et al.*, 2004] to simpler estimates of macroscopic averages of bedload transport parameters. Within this range are models that combine a) the statistics extracted from a saltation model for individual grains with b) a macroscopic condition to determine the mean volume per unit area of particles in bedload transport, to derive a macroscopic relation for bedload transport [see e.g., *Wiberg and Smith* ,1989; *Sekine and Kikkawa* ,1992; *Niño and García*, 1994]. However, no one method or relation developed has universal application [*Gómez and Church*, 1989; *Yang and Huang*, 2001; *Barry et al.*, 2004]. It is likely that successful modeling of bedload transport will depend on improved physical

descriptions of the mechanics of entrainment, transport and deposition of bed particles. We argue that such improvements can be achieved through experimental work with tracer stones.

The results and analysis of experiments using tracer stones are presented in this paper. Experiments were conducted under conditions of equilibrium lower-regime plane-bed bedload transport of uniform gravel, in a straight sediment-fed flume with rectangular cross-section, constant width and inerodible walls. Experiments were designed to simplify the problem as much as possible. Use of uniform sediment allows characterization of tracer displacement without the complications associated with multiple grain sizes [*Bridge and Dominic*, 1984; *Tsujimoto*, 1990; *Church and Hassan*, 1992; *Hassan et al.*, 1992; *Buffington and Montgomery*, 1999; *Sun and Donahue*, 2000; *Blom and Parker*, 2004]. Experimental conditions also precluded complications associated with the formation of dunes, alternate bars and pool-riffle sequences [*Keller and Florsheim*, 1993; *Lisle et al.*, 1993; *Carling and Wood*, 1994; *Sear*, 1996; *Ferguson et al.*, 2002; *Haschenburger and Wilcock*, 2003; *Pyrce and Ashmore*, 2003, 2005]. These simplifications were appropriate because tracer displacement, even under very simple conditions, is not adequately understood. As *Hassan and Ergenzinger* [2002] point out, "Although considerable attention has been paid to specific influences that are known to determine river sediment transport rates and patterns, there still is a large inconsistency between data collected in the field and the results of theoretical and empirical models."

Here the characteristic displacement patterns of tracer stones are linked to stochastic temporal variations in bed elevation at different streamwise locations in the flume. Measurements were conducted for various combinations of constant water discharge and sediment feed rate. Experimental results led to the derivation of predictor functions for the statistics of bed elevation fluctuations, particle entrainment rates, particle virtual velocities and

particle step lengths. These allowed quantification of: (i) a relation between the vertical position of a particle in the bed deposit, its frequency of entrainment and associated bedload transport rate; and (ii) a relation between the streamwise displacement of a particle, duration of competent flow and associated bedload transport rate.

2. Background

A common approach for estimating the bedload transport rate in a stream is the use of empirically derived relations based on the mean characteristics of the driving force (e.g., discharge, flow velocity, water depth, friction slope), and corresponding resistance properties of the bed (e.g., grain size distribution, density of the sediment, bed structure, bedforms, or channel morphology). Such relations predict a macroscopic bedload transport rate that is averaged over fluctuations associated with entrainment and deposition of bed particles. Some examples of this approach are the relations of *Meyer-Peter and Müller* [1948], *Fernández Luque and van Beek* [1976], *Parker* [1990], and *Wilcock and Crowe* [2003]. All terms in these relations are deterministic and represent values averaged over stochastic fluctuations.

Macroscopic bedload transport relations are linked to the Exner equation of sediment continuity to describe the morphodynamic evolution of a river. In the case of sediment mixtures, models have been developed which not only describe the evolution of bed elevation, but also of the grain size distribution of sediment in the bed [*Hirano*, 1971; *Borah et al.*, 1982; *Misri et al.*, 1984; *Ribberink*, 1987; *Bridge and Bennett*, 1992; *Armanini*, 1995; *Parker et al.*, 2000]. Monte Carlo simulations are useful for evaluating the sensitivity of transport relations to input variables [*Wilcock*, 2004]. Such modeling, however, remains poorly linked to the underlying, intrinsically stochastic processes of particle entrainment, streamwise displacement and deposition which

drive bedload transport, in part because of limited descriptions of the large variability inherent in particle motion.

The classical macroscopic deterministic approach has at least two drawbacks [*Parker et al.*, 2000]. First, such models do not contain the mechanics necessary to describe the disposition of individual particles, and hence do not explicitly account for the possibility of vertical or longitudinal sorting of bed material and the corresponding effect on the overall morphodynamic evolution of the stream. *Lisle et al.* [2000] indicate no perfect match between flow strength (e.g., bed shear stress, or stream power) and bed composition and configuration can be found at the local scale. Other authors [*Tsujimoto and Motohashi*, 1990; *Buffington and Montgomery*, 1999; *Hassan and Church*, 2000; *Cao and Carling*, 2002; *Nelson et al.*, 2002; *Blom*, 2003] note that the classical approach is somewhat deficient in terms of a process-oriented coupling of the governing equations linking flow momentum, sediment transport and bed sediment continuity.

Second, it has been well established that the entrainment, transport and deposition of bed particles are all stochastic in nature [*Einstein*, 1950; *Hubbell and Sayre*, 1964; *Paintal*, 1971; *Nakagawa and Tsujimoto*, 1980; *Schmidt and Ergenzinger*, 1992; *Habersack*, 2001], due to the turbulent characteristics of the flow velocity near the bed and the random exposure and support conditions of individual bed particles [*Nakagawa and Nezu*, 1977; *Roy et al.*, 1996; *Shvidchenko and Pender*, 2000; *Papanicolaou et al.*, 2002; *McEwan et al.*, 2004].

Tracer stones facilitate the evaluation of both stochastic and macroscopic processes. A reasonable hypothesis is that their vertical and streamwise displacement history serves as a good indicator of the bedload transport response of a stream to given water discharge and sediment supply conditions [*Wilcock*, 1997b; *Haschenburger and Church*, 1998; *DeVries*, 2000; *Sear et al.*, 2000; *McNamara and Borden*, 2004]. To evaluate this, the movement of an individual gravel

bed particle can be discretized into three phases: (i) the particle is exposed on the surface of the bed, (ii) it is entrained into transport by the flowing water, and (iii) it is detrained from the flow and deposited back onto the bed. Two points should be emphasized, however. First, the three phases do not necessarily occur sequentially one immediately after the other, as some time in a resting position can be expected between phases (i) and (ii), as well as between (iii) and (i) [*Crickmore and Lean*, 1962a; *Hassan and Church*, 1994]. Recognition of this fact has led to the definition of a particle virtual velocity [*Einstein*, 1937], which represents the average particle velocity including both periods when the particle is in motion and when it is at rest, either on the bed surface or buried beneath it [*Bridge and Dominic*, 1984; *Hassan et al.*, 1991; *Niño et al.*, 1994; *Wu and Yang*, 2004]. Second, particle entrainment, transport and deposition are stochastic processes. Therefore, rather than representing these processes in terms of their mean values, a more detailed characterization should include the probability density functions of possible values [*Crickmore and Lean*, 1962b; *Hassan et al.*, 1991].

Under steady and uniform transport conditions, bedload particles constantly but sporadically interchange with the bed. Once entrained into motion, a moving particle is eventually deposited on the bed surface or buried, where it may remain for a substantial amount of time. Fluctuations in bed elevation may cause the grain to be exhumed and re-entrained, however, such that the three motion phases can begin again.

3. A unifying structure for bedload transport encompassing tracers

Three alternative forms of the bedload sediment continuity equation for equilibrium conditions are introduced below. All three involve macroscopic parameters (i.e., parameters that have been averaged over stochastic fluctuations). The first of these relations considers continuity

of moving bedload particles. Let q_b denote the volume bedload transport rate per unit width; U_{bm} denote the mean velocity of moving bedload particles; and ξ_b denote the volume of particles in bedload motion per unit bed area. Conservation of mass of bedload particles implies:

$$q_b = \xi_b U_{bm} \tag{1}$$

Relations of this form have been used e.g. by *Wiberg and Smith* [1989], *Sekine and Kikkawa* [1992], *Niño and García* [1994] and others to obtain bedload transport relations of the form:

$$q^* = f\left(\tau^*\right) \tag{2}$$

where q^* is the dimensionless bedload transport rate, or Einstein number; and τ^* is the dimensionless bed shear stress, or Shields number. These numbers are given as:

$$q^* = \frac{q_b}{\sqrt{RgD_{50}}D_{50}} \tag{3}$$

$$\tau^* = \frac{\tau_b}{\rho RgD_{50}} \tag{4}$$

where τ_b is the bed shear stress; g is the acceleration of gravity; ρ is the density of water; D_{50} is the median particle size of the bed sediment (the only size needed to characterize the uniform sediment considered here); and R is the submerged specific gravity of the sediment, given as:

$$R = \frac{\rho_s}{\rho} - 1 \tag{5}$$

where ρ_s is the density of sediment. The use of equation (1) is problematic, however, because of the difficulty in deriving a suitable, practical expression of U_{bm} that describes rolling, sliding and saltation [*DeVries*, 2000].

A second conservation relation, first introduced by *Einstein* [1950], takes the form:

$$q_b = E_b L_s \tag{6}$$

where E_b is the volume rate per unit bed area at which particles are entrained from the bed into bedload motion; and L_s is the step length, or distance a particle moves before being redeposited. This relation has been used by *Nakagawa and Tsujimoto* [1976], and more recently by *Wilcock* [1997b] and *McEwan et al.* [2004], to develop bedload relations of type of equation (2). This relation is difficult to evaluate because of the difficulty in defining L_s in a way that can be measured consistently.

It is the third conservation relation considered here that takes advantage of the use of tracer stones. Any given particle is assumed to have some virtual velocity U_{pir}, which includes the time the particle is in motion with mean velocity U_{bm} and the time the particle is at rest. It is assumed that the particle may be at rest either on the bed surface, or while temporarily buried in the bed within a layer of thickness L_a that may be termed the active layer [*Hirano*, 1971]. The active layer represents the thickness of bed sediment that is constantly reworked by scour and fill, even at macroscopic mobile-bed equilibrium. Bedload continuity thus takes the form:

$$q_b = U_{pir} L_a \tag{7}$$

The term U_{pir} is determined by sequential measurements of the distance moved by a tracer stone. The term L_a is evaluated by quantifying the exhumation of tracer stones buried at various depths within the bed. Experiments for evaluating these terms also allow determination of a standard bedload transport relation of the form of (2).

4. Flume experiments

4.1 Layout

The physical modeling of bedload transport processes in gravel-bed streams was carried out in a flume located at St. Anthony Falls Laboratory (SAFL), University of Minnesota. The

general arrangement of the experimental facility included: (i) a 0.5-m wide, 0.9-m deep, 27.5-m long, straight flume of rectangular cross-section and smooth metallic walls; (ii) a regulated water supply with maximum flow rate of 0.120 $m^3 s^{-1}$ calibrated with a rectangular sharp-crested weir located at the downstream end of the head tank; (iii) pressure tubes (piezometers) used to measure water surface levels, which were placed every 0.5 m in the streamwise direction, between 2.0 and 20.0 m downstream from the entrance weir; (iv) controlled gravel supply at the upstream end of the test reach, via an auger-type sediment feeder, for a maximum feed rate of 0.150 kg s^{-1}; and (v) automated recirculation of the gravel collected in a sediment trap at the downstream end of the flume, from where it was jet-pumped back (with a gravel eductor) to a buffer containment box installed above the sediment feeder. Due to the presence of the sediment feeder, the system operated as a sediment-fed flume rather than a sediment-recirculating flume. The test reach had a length of 22.5 m, as measured from the upstream weir to the downstream sediment trap. We use the term "streamwise position" to define the distance downstream from the entrance weir.

Two point gauges were used to measure longitudinal bed profiles. In addition, a sonar-transducer system was used to record bed elevation fluctuations simultaneously at five fixed streamwise positions, with a measurement interval of 3 s. All ultrasonic transducer probes were of videoscan immersion type, with a nominal element size of 1 in (25.4 mm). Three of these operated at a frequency of 0.5 MHz and the other two at 1.0 MHz. The near field distance and beam angle of the 0.5 MHz-type probes were 55 mm and 6.9º, respectively; corresponding values for the 1.0 MHz-type probes were 109 mm and 3.4º. Independent measurements with the same sonar system in standing water and a fixed gravel bottom surface resulted in a standard deviation of signal fluctuations (i.e., the measurement error) of 0.16 and 0.04 mm for the

0.5 MHz- and 1.0 MHz-type probes, respectively. The primary issues with installing the ultrasonic probes were related to avoiding entrainment of air bubbles below them, while keeping their bottom as far as possible from the gravel bed, hence minimizing their effect on the local flow field and bed material entrainment.

The sediment used in all experiments was well-sorted gravel, with geometric mean particle size D_g = 7.2 mm, geometric standard deviation σ_g = 1.2, median particle size D_{50} = 7.1 mm, particle size for which 90% of the sediment is finer D_{90} = 9.6 mm, and density ρ_s = 2550 kg m^{-3}. Passive tracer stones selected from this sediment were used to study the vertical and streamwise dispersion of individual bed particles. Tracers were marked by painting the gravel particles with spray paint, indelible color pens or a combination of both. Sixteen groups of tracers were formed, each a distinct color or combination of colors including: orange, red, blue, yellow opaque, fluorescent yellow, green, pink, orange-black, red-black, green-purple dot, pink-purple dot, light green-orange, yellow opaque-green, fluorescent yellow-purple, fluorescent yellow-orange and fluorescent yellow-brown. About 200 tracer stones from each group were used for a total of approximately 3200 tracers per experiment.

A second flume was used for complementary experiments on bedload transport processes. This flume was also located at SAFL, University of Minnesota. Its layout was similar to that of the first experimental facility described above. There were two differences: (i) the test reach had a length of 8.0 m; and (ii) the flume had glass walls. This shorter flume served to augment data used to derive an empirical bedload transport relation. Experiments in this second flume yielded preliminary estimates of the number of layers of tracer stones that must be installed to define, for the range of water discharges and sediment feed rates, the thickness of the active layer. However, none of the data collected in this second facility with regard to tracer displacements were used

here: the flume was so short that once tracer stones were entrained, most if not all were displaced all the way to the sediment trap, such that no precise travel distances could be obtained.

4.2 Procedures

The general sequence of experiments reported here included: (i) running the flume long enough to achieve lower-regime plane-bed normal (uniform and steady) flow equilibrium transport conditions, for constant values of water discharge and sediment feed rate; (ii) excavating the bed deposit at four locations and carefully replacing extracted sediment with distinctly colored layers of tracer stones; (iii) re-running the experiment for a predetermined duration with the same combination of water discharge and sediment feed rate as above; and (iv) measuring the final location of tracers after completion of each experimental run. This sequence was repeated eight times for ten (10) different equilibrium states and run durations. Each step is explained in greater detail below.

The time required to attain lower-regime plane-bed equilibrium transport depends on, among other things, the initial bed slope, water discharge, and sediment feed rate. It took approximately 30 to 50 hours to achieve equilibrium conditions, which were defined by constant (in time and space) streamwise water surface and bed slopes. Water surface slope was measured by the aforementioned piezometers, while bed slope was measured between streamwise positions 4.0 and 18.0 m. In addition, water levels were frequently recorded, the elevation of gravel in the buffer box of the sediment feeder was monitored to ensure steady state, and three bed profiles were obtained every half day to validate equilibrium conditions. Surveys of the bed profile included measuring bed elevations every 0.5 m in the streamwise direction, between positions 2.0 and 20.0 m, at three locations on each cross-section: at 0.12 m from the right wall (looking

downstream), at the channel center and at 0.12 m from the left wall of the flume. The absence of bedforms was verified during these surveys.

Once mobile-bed equilibrium was achieved, simultaneous measurements of bed elevation were recorded with the sonar-transducer system at five streamwise positions (6.75, 7.75, 8.75, 12.75 and 16.75 m). The distance between the bottom of the ultrasonic probes and the mean bed surface was neither constant for all probes nor for all experiments. The corresponding beam spread (footprint) thus varied by probe and experiment as well. The minimum, average and maximum footprint for the 0.5 MHz-type were 4.6, 7.2 and 10.1 mm, respectively; whereas for the 1.0 MHz-type it was 2.4, 3.8 and 4.9 mm, respectively. Hence, the maximum footprint of the sound wave was about the size of D_{90}. All sonar measurements were done in 3 s intervals, and produced time series data of 1-hr duration for each of the five streamwise positions.

Local excavation of sediment and replacement with an equivalent volume of tracer stones was conducted in four locations: at 6.75 m from the entrance weir at 0.17 m from the right and left walls of the flume, and at 7.75 and 8.75 m at the center of the flume. The bed elevation at these distances was monitored with the sonar-transducer system. Measurements of high temporal resolution were also done prior to seeding with tracer stones. Each excavation had a surface area of 0.10 x 0.10 m, and a depth of approximately 3.0 to 3.5 cm, or approximately 4 D_{50} to 4 D_{90}. A serrated metal casing was used to define the excavation area. A teaspoon was employed to extract sediment, while working the metal casing downward to the target elevation depth. The bottom surface of each excavation was leveled with a metal sheet and then surveyed with a point gauge. A layer of tracers of given color was installed, leveled and surveyed to determine the thickness of each layer, and then the casing was readjusted to the new surface. This procedure continued until four layers of tracers were installed at each location, each containing about

200 tracer stones. Here the "*first*" layer is defined as the exposed layer flush with the bed surface. The "*second*", "*third*" and "*fourth*" layers are respectively the layers sequentially buried below the *first*. The distinct color of each layer thus served as a proxy for initial burial depth or vertical location and also streamwise position in the bed deposit.

Once tracers were seeded the experiment began again by filling the flume tank slowly with water. This was done to avoid any initial artificial over-entrainment of tracers. Water discharge was then gradually increased up to the experimental value, and the sediment feeder was turned on. Tracers displaced beyond the constraints of the system were picked out of the buffer box, so that the results were not confounded by painted particles that made more than one trip through the flume. Eight different and independent runs were completed for each equilibrium state. The durations of the first six runs were the same for all equilibrium states: 1, 2, 15, 30, 60 and 120 minutes. The last two runs in each equilibrium state, referred to here as "*Short-1*" and "*Short-2*", were of variable duration (see Table 1) determined by the following criteria: (i) *Short-1* would be of sufficient duration to permit the displacement of as many tracers as possible, but restricting the number of painted particles moving out of the system to less than 10% of the total displaced; and (ii) *Short-2* would have a duration equal to twice that of *Short-1*. A preparation run without tracers, following a similar procedure to the one described in step (i), was performed in between each of the runs with tracers; it lasted between 8 and 12 hours before proceeding with step (ii).

The final locations of tracer stones were used to place them into one of four classes where "*SD*" denotes streamwise displacement: (i) "*SD1*" is the class of tracers that did not move from their initial seeding position; (ii) "*SD2*" is the class of tracers entrained into bedload transport and displaced out of the system; (iii) "*SD3*" is the class of tracers entrained into bedload

transport, displaced upstream of the sediment trap and found on the bed surface; and (iv) "*SD4*" is the class of tracers entrained into bedload transport, displaced upstream of the sediment trap and found buried in the bed deposit. Identification involved counting the number of tracers of every color that corresponded to each of the four classes above and recording the streamwise position of particles in *SD3* and *SD4*; the latter was not performed for runs of 1- and 2-minute duration. Tracer recovery always exceeded 99%, with less than 0.25% loss during most experiments. All lost tracers were recovered during the preparation run for the next experiment.

4.3 Results

Table 2 is a summary of reach-averaged conditions of the 10 experimental states, once lower-regime plane-bed equilibrium conditions were achieved. This table includes values of constant water discharge Q_w, sediment feed rate Q_{bf}, streamwise bed surface slope S_0, streamwise water surface slope S_w, and water depth H. The values of S_0 and S_w were almost identical for a given equilibrium state. Furthermore, bed surveys indicated the absence of dunes, ripples and alternate bars, and when bars occasionally formed they remained subtle features. For example, Figure 1 shows the measurements for Run 9, in which the variations in bed elevation at any given cross-section were smaller than D_{90}.

The algorithm developed to process raw data obtained with the sonar-transducer system discriminated between particles in bedload motion and actual bed elevation. Two time series of bed elevation are presented in Figure 2. The time series are plotted for the five fixed streamwise positions where ultrasonic probes were located. Figure 2a shows measurements corresponding to a relatively low bedload transport rate (Run 10), while Figure 2b corresponds to a relatively high bedload transport rate (Run 8). It is evident the magnitude of fluctuations in bed elevation

increases from the case depicted in Figure 2a to that in Figure 2b, even though the equilibrium streamwise slope is about the same in both cases (see Table 2). The increase in flow strength, represented here by the bed shear stress, appears to be driving the increase in fluctuations.

The number of tracer stones displaced was recorded by color. Consequently, the fraction of tracer stones entrained within each color could be calculated for a given test duration. When estimating particle entrainment rates, no distinction is needed between groups *SD2*, *SD3* or *SD4*, as all particles in these classes were entrained regardless of their initial and ultimate positions. Figure 3a shows the fraction of tracers displaced from each layer as a function of time. Of particular interest were the conditions of Run 9, which corresponds to a relatively low bedload transport rate (see Table 2). Conversely, Figure 3b presents results for a relatively high bedload transport rate (Run 2). A comparison of Figure 3a and Figure 3b reveals that experiments conducted at SAFL allow direct measurement of elevation-specific particle entrainment. The main results show the longer the duration of competent flow and/or the larger the flow strength, the larger the fraction of tracer stones displaced and the deeper the layer accessed. For a given equilibrium state, however, it is expected that the total and elevation-specific particle entrainment rates should be independent of duration of competent flow. This issue is resolved in the next section of the paper.

Precise information is available for the travel distance of displaced tracer stones in class *SD3* and *SD4* (i.e., stones displaced within limits of the flume). Statistics for displacement were computed without taking into account group *SD2* (tracers displaced out of the flume). Using data from *SD2* underestimate actual travel distances that would be obtained in the case of an infinitely long flume. The issue of distributions obtained from truncated statistics is resolved in the next section of the paper.

We explored the influence of the vertical reworking of the bed deposit on particle streamwise travel distances by classifying the tracers in groups *SD3* and *SD4*. We begin by dividing the total number of painted particles in groups *SD3* and *SD4* into the following four classes: (i) tracers seeded on the bed surface, displaced and found buried within the bed; (ii) tracers seeded on the bed surface, displaced and found on the bed surface; (iii) tracers seeded buried within the bed, displaced and found buried within the bed; and (iv) tracers seeded buried within the bed, displaced and found on the bed surface. The mean travel distance was computed for each of these four classes, and using the corresponding test duration, the mean particle virtual velocities were computed. Figure 4 illustrates the results of such calculations for Runs 11 and 4, a relatively high and low bedload transport rate, respectively (see Table 2). Calculations were performed for the two shortest durations for which travel distances were recorded (*Short-1* and *Short-2*), and for which the number of painted particles in group *SD2* was a minimum. Figure 4 shows several interesting features: a) particle virtual velocities increase with flow strength for any of the four classes, b) there is no definitive correlation between particle virtual velocity and duration of competent flow for a given equilibrium state (recall that the effect of the tracers in group *SD2* is not quantified here), and c) particle virtual velocities for tracers that were found at the bed surface are higher than for those found within the bed. A complete analysis of all experimental results is presented in the next section of this paper.

5. Data analysis and interpretation

5.1 Bedload transport relation

An empirical bedload transport relation was derived based on flume experiments conducted at SAFL. The relation for Shields number τ^* for sediment mobility calculations derived from (4) and the normal flow assumption is given as:

$$\tau^* = \frac{HS_0}{RD_{50}} \tag{8}$$

The Einstein number q^* was related to the Shields number τ^* by regression, assuming a priori an exponent of 1.50:

$$q^* = 2.66\left(\tau^* - 0.0549\right)^{1.50} \tag{9}$$

Experimental data and volume bedload transport predictor are plotted in Figure 5. Values of Shields number τ^* were not determined directly from (8), but corrected to remove sidewall effects following the procedure of Vanoni and Brooks [*Vanoni*, 1975]. The "critical" Shields number τ^*_{cr} = 0.0549, obtained in the best fit of this relation is very close to the value of 0.0550 computed using the relation proposed by *Yalin and Scheuerlein* [1988].

Equation (9) is not proposed as a new, universal predictor of the volume bedload transport rate of uniform gravel under lower-regime plane-bed equilibrium conditions. Rather, it serves as a baseline relation to analyze tracer displacement.

5.2 Bed elevation fluctuations

Bed elevation at a point fluctuates in time under mobile-bed equilibrium. The experiments reported here demonstrate this for even the simplest case of lower-regime plane-bed equilibrium bedload transport of uniform gravel. These fluctuations occur at time scales shorter than those

associated with overall net bed aggradation or degradation, and at mobile-bed equilibrium they do not constitute a permanent departure from the expected mean bed profile. Local stochastic imbalances in the bedload transport rate, and/or instantaneous disequilibrium between particle deposition and entrainment rates, are the causes of time variations in bed elevation. *Armanini* [1995], for example, hypothesized that these fluctuations are due in part to large scale turbulence. Stochastic bed elevation fluctuations can be characterized by a probability density function that is unique for given mobile-bed equilibrium conditions [*Marion et al.*, 2003]. The following paragraphs expand on how this was done for these data.

The time series of bed elevation fluctuations were converted into time series of bed elevation deviations from the corresponding mean bed elevation for the five streamwise positions where sonar measurements were conducted using:

$$y = \eta - z \tag{10}$$

where y denotes the deviation from mean bed elevation; η denotes the mean bed elevation; and z denotes the instantaneous bed elevation. Coordinate y is positive downward in (10) and is boundary-attached to the mean bed elevation η. Computation of y was performed for time scales sufficiently long to define a representative mean value η yielding an average value $\overline{y} = 0$. For a given equilibrium state, the time series obtained at the five recording positions were aggregated into a single dataset. This dataset was used to compute the standard deviation of bed elevation fluctuations s_y:

$$s_y = \left[\sum_{i=1}^{N} \frac{y_i^2}{(N-1)} \right]^{1/2} \tag{11}$$

where y_i is the ith value of the bed elevation deviation y from the mean bed elevation η; and N is the size of the dataset. Working with the aggregated time series of bed elevation fluctuations y,

which all together correspond to a time scale sufficiently larger than that associated with the fluctuations, an empirical cumulative distribution was constructed for each equilibrium state. A normal distribution model provided an excellent fit to these empirical distributions. Two examples of goodness of fit are illustrated in Figure 6, where both the empirical and the theoretical cumulative distributions functions are depicted. The agreement is remarkably good for almost the entire range of potential bed elevation deviation values, with the exception of the extreme tails of the distribution. Thus, the probability density function of bed elevation fluctuations $p_e(y)$ is given as:

$$p_e(y) = \frac{1}{\sqrt{2\pi}s_y}\exp\left[-\frac{1}{2}\left(\frac{y}{s_y}\right)^2\right] \tag{12}$$

Pender et al. [2001] found that the empirical probability density function of spatial (rather than temporal) bed elevation fluctuations was bell-shaped even in the case of a degrading bed composed of poorly sorted sediment. The earlier experimental work of *Crickmore and Lean* [1962a, 1962b] in a 100-m long flume with transport over a sand bed covered with ripples suggested that the spatial (rather than temporal) bed elevation fluctuations around the mean bed elevation profile followed a normal distribution.

A physical interpretation of the meaning of $p_e(y)$ is obtained from Figure 7, where a line is traced at relative level y, parallel to the mean bed elevation η. Let $P_S(y)$ denote the fraction of sediment (and pores) at elevation y. For time scales shorter than those corresponding to overall net bed aggradation or degradation, it can be argued that: (i) $P_S(y \to -\infty) = 0$, i.e. there is no sediment far above the mean bed η; (ii) $P_S(y \to +\infty) = 1$, i.e. deep in the deposit there is nothing but sediment and pore space; and (iii) $P_S(y)$ is a monotonically increasing function. The combination of these three conditions resembles the definition of a cumulative distribution

function, in this case of the sediment (and pores) at relative level y. In a more physical context, $P_S(y)$ can be interpreted as the probability that the instantaneous relative bed elevation is less than or equal to y. Thus, its associated probability density function of relative bed elevation is $p_e(y)$, which by definition is given as:

$$p_e(y) = \frac{\partial P_S(y)}{\partial y} \tag{13}$$

$p_e(y)$, already defined in (12) for the cases of mobile-bed equilibrium dealt with here, satisfies:

$$\int_{-\infty}^{+\infty} p_e(y)\,dy = 1 \tag{14}$$

and its variance s_y^2 is given as:

$$s_y^2 = \int_{-\infty}^{+\infty} y^2 p_e(y)\,dy \tag{15}$$

The mean value $\overline{y}$ is:

$$\overline{y} = \int_{-\infty}^{+\infty} y p_e(y)\,dy = 0 \tag{16}$$

The form of (12) indicates that the only variable required for defining the distribution of bed elevation fluctuations is its standard deviation s_y. The magnitude of s_y should scale with the characteristic bed particle size under equilibrium transport conditions because it reflects alternately the occupation and evacuation of space by individual particles. In addition, depending on the transport rate and sampling time, the magnitude of s_y should reflect short-term lowering and raising of the bed everywhere in the vicinity of the bed elevation measurement in response to subtle, local transport rate imbalances. Accordingly, we may define a dimensionless standard deviation $\hat{s}_y$ as:

$$\hat{s}_y = \frac{s_y}{D_{50}} \tag{17}$$

Our data relate $\hat{s}_y$ and the (sidewall-corrected) Shields number τ^* through:

$$\hat{s}_y = 3.09\left(\tau^* - 0.0549\right)^{0.56} \tag{18}$$

The form of (18) is consistent with Figure 2; a larger flow strength, here quantified in terms of a larger Shields number, leads to more intense bed elevation fluctuations. As the bed elevation fluctuations increase, the probability that a relatively deeply buried particle is exposed increases. Even at mobile-bed equilibrium, increased fluctuations in bed elevation can create conditions under which particles that are buried relative to the mean bed are exposed and entrained. By the same token, these fluctuations provide a mechanism for burying particles completely below the mean bed level. Equation (18) indicates that a higher Shields number could drive a faster exchange process.

The concept of an active layer thickness L_a was introduced in the context of tracers in (7). There is no precise definition of the active layer thickness, because the concept is statistical [*Parker et al.*, 2000]. It can, however, be defined as follows. Let y_a denote a position in the bed such that the cumulative distribution function P_{sa} at y_a attains a value appropriately close to unity. Then L_a is the average thickness of bed material (sediment and pores as opposed to flowing water above) between $y = -\infty$ and $y = y_a$, which is given in *Parker et al.* [2000; equation 19] as:

$$L_a = \int_{-\infty}^{y_a} P_S\left(y\right) dy \tag{19}$$

Let $\hat{L}_a$ denote the dimensionless thickness of the active layer, given as:

$$\hat{L}_a = \frac{L_a}{D_{50}} \tag{20}$$

Assuming that $\hat{L}_a$ scales linearly with $\hat{s}_y$, then:

$$\hat{L}_a = \alpha \hat{s}_y \tag{21}$$

where α is an order-one scaling coefficient. Hence, a value of $P_{sa} = 0.95$, for example, combined with the normally distributed $p_e(y)$ yields a value of α in (21) of 1.62, so that:

$$L_a = 1.62 s_y \tag{22}$$

In general:

$$L_a = \alpha\left(P_{sa}\right) s_y \tag{23}$$

where α is now a function of P_{sa}.

Let $\hat{U}_{pir}$ denote the dimensionless particle virtual velocity, given as:

$$\hat{U}_{pir} = \frac{U_{pir}}{\sqrt{RgD_{50}}} \tag{24}$$

Combining (3), (7), (9), (17), (18), (23) and (24) yields the following predictor function in terms of the (sidewall-corrected) Shields number τ^*:

$$\hat{U}_{pir} = \frac{0.86}{\alpha\left(P_{sa}\right)}\left(\tau^* - 0.0549\right)^{0.94} \tag{25}$$

Appropriate values for P_{sa}, and thus $\alpha(P_{sa})$, are specified below. Comparison of predictor functions (18) and (25) indicate that the rate of increase of $\hat{U}_{pir}$ with Shields number is larger than that of $\hat{s}_y$. In other words, an increase in bedload transport rate causes the particle virtual velocity to increase at a greater rate than the thickness of the surface layer of the bed deposit that is active during a transport event. This result may be tentatively applied to the case of mobile-

bed equilibrium in a stream with bed composed of size mixtures. It suggests that sediment sorting might be more evident in the streamwise direction than in the vertical. These observations are consistent with *DeVries* [2002], who using field measurements in ten gravel bed streams in the Pacific Northwest USA, found an increase in the bedload transport rate was due primarily to an increase in the fraction of bed surface mobilized and grain velocity, rather than an increase in the thickness of the moving bedload layer.

5.3 Particle entrainment and deposition

Figure 8a illustrates the fraction of painted particles (with respect to total seeded) entrained in each experiment for which the run duration was 15 minutes. The fraction of tracers moved per layer increases with excess shear stress as does the effective depth of tracers subject to entrainment. Tracer stones in the top two layers were the only stones displaced in the six runs of smaller excess shear stress, whereas tracer stones as deep as the *fourth* layer were moved in runs of larger excess shear stress. Figure 8b corresponds to experiments for which the run duration was 120 minutes. Similar trends occur here as well, with the fraction of tracers moved in the *third* and *fourth* layers as large as 0.59 and 0.24, respectively. Figure 8a and Figure 8b show that the fraction of tracers moved per layer increases with run duration. The observed effect of duration may reflect the value of L_a being proportional to predominantly grain size in short runs, and to the net sum of grain size plus spatially averaged change in bed elevation in longer runs.

In many morphodynamic models of gravel-bed streams that use the active layer concept [*Hirano*, 1971], the active layer is prescribed solely in terms of the grain size distribution of the bed surface material (typically expressed as a multiple of D_{90}). The results of Figure 8a and

Figure 8b combined with (17), (18) and (22), however, indicate that the thickness of the active layer also scales with the strength of the flow, as parameterized in terms of the Shields number.

The entrainment rate should be independent of run duration. Given that the analysis herein is for equilibrium bedload transport under uniform and steady flow conditions, the entrainment formulation of mass continuity can be applied to any region of the bed deposit. If the region corresponds to one occupied by tracer stones, then:

$$z_{tr}\frac{df_{bti}}{dt} = D_{tr} - E_{tr} \tag{26}$$

where z_{tr} is the thickness of the zone occupied by tracers; f_{bti} is the fraction of tracers in control volume at time t; D_{tr} is the volume deposition rate of tracers per unit bed area; and E_{tr} is the volume entrainment rate of tracers per unit bed area.

In experiments reported here, no tracers were supplied from upstream of the region where the tracers were initially placed, so within this region:

$$D_{tr} = 0 \tag{27}$$

The parameter E_{tr} is further specified as:

$$E_{tr} = E_{btt} f_{bti} \tag{28}$$

where E_{btt} is the volume entrainment rate of sediment per unit bed area. Equation (26) becomes:

$$z_{tr}\frac{df_{bti}}{dt} = -E_{btt} f_{bti} \tag{29}$$

The implicit assumption in this mass balance is that z_{tr} is large enough to cover the depth of bed deposit subject to entrainment and deposition. Integrating equation (29) from time t_1 to t_2 yields:

$$E_{btt} = -\frac{z_{tr}}{(t_2 - t_1)}\ln\left[\frac{f_{bti}(t_2)}{f_{bti}(t_1)}\right] \tag{30}$$

E_{btt} was calculated from data obtained from the 8 different test durations. E_{btt} was calculated for each layer of tracer stones installed by using the average estimate obtained from the allowable (maximum) 36 different combinations of t_1 and t_2 (with $t_2 > t_1$). The average estimate was selected as it is less biased to potential over- or under-estimation of entrainment rates in runs of specific duration. For a given equilibrium state, the total particle entrainment rate E_b is obtained by vertical integration of the measured layer-specific entrainment rates. The entrainment rate of a given layer, however, must be normalized with the fraction of time the bed surface is actually at that layer.

Let $p_{Ent}(y)$ denote the probability density function that a particle entrained from the bed into bedload transport comes from a depth y relative to the mean bed elevation η, and $p_{Dep}(y)$ denote the probability density function that a bedload particle is deposited onto the bed at a depth y relative to the mean bed elevation η. These definitions are completed by indicating that $E_b\, p_{Ent}(y)\, \Delta y$ represents the entrainment rate from level y; $D_b\, p_{Dep}(y)\, \Delta y$ represents the deposition rate at level y; and D_b is the volume rate of particle deposition per unit bed area. By definition:

$$\int_{-\infty}^{+\infty} p_{Ent}(y)\, dy = 1 \tag{31}$$

$$\int_{-\infty}^{+\infty} p_{Dep}(y)\, dy = 1 \tag{32}$$

Thus, $E_b\, p_{Ent}(y)$ and $D_b\, p_{Dep}(y)$ represent the elevation-specific entrainment and deposition rates, respectively. Let

$$p_{Ent}(y) = p_B(y - y_{bE}) \tag{33}$$

$$p_{Dep}(y) = p_B(y - y_{bD}) \tag{34}$$

where $p_B(y)$ is a normalizing probability density, which is not necessarily equal to the probability density $p_e(y)$ of bed elevation fluctuations; y_{bE} is the offset distance from the mean bed (at $y = 0$) for the entrainment function; and y_{bD} is the offset distance from the mean bed (at $y = 0$) for the deposition function. Our experiments allow quantification of only the offset y_{bE} at equilibrium conditions. Assumed that y_{bE} and y_{bD} can be decomposed as:

$$y_{bE} = y_0 - y_1 \tag{35}$$

$$y_{bD} = y_0 + y_1 \tag{36}$$

hence, (33) and (34) become:

$$p_{Ent}(y) = p_B(y - y_0 + y_1) \tag{37}$$

$$p_{Dep}(y) = p_B(y - y_0 - y_1) \tag{38}$$

Equations (37) and (38) allow a) the probability densities of entrainment and deposition to differ from that of elevation fluctuation, b) these same densities to be offset relative to the mean bed elevation ($y = 0$) [see e.g., *Crickmore and Lean*, 1962a], and c) these same densities to be offset from each other by an amount $2\,y_1$.

The data allow estimation of an exponential form of the probability density function $p_{Ent}(y)$ at equilibrium conditions:

$$p_{Ent}(y) = \frac{1}{2s_y}\exp\left(-\frac{|y - y_0 + y_1|}{s_y}\right) \tag{39}$$

where y_0 is an offset characterizing mobile-bed equilibrium; and y_1 is an additional offset that may be generated by non-equilibrium conditions. For our mobile-bed equilibrium experiments

$$y_0 = 0.25D_{50} \tag{40}$$

Accordingly, we hypothesize the form of $p_{Dep}(y)$ to be exponential:

$$p_{Dep}(y) = \frac{1}{2s_y} \exp\left(-\frac{|y - y_0 - y_1|}{s_y} \right) \tag{41}$$

where y_0 is given in (40). A positive value of the offset y_1, characterizing disequilibrium conditions, is hypothesized to bias deposition toward lower elevations and entrainment toward higher elevations. Determination of a functional relationship for y_1 awaits experimental results for disequilibrium conditions. The entrainment function $p_{Ent}(y)$ in (39) is continuous in y, thus overcoming the step function approximation of the active layer formulation [*Hirano*, 1971; *Parker et al.*, 2000]. $p_{Ent}(y)$ depends on the standard deviation s_y of bed elevation fluctuations, hence from (17) and (18) it correlates not only with the median particle size but also with the (sidewall-corrected) Shields number.

Our experimental data for mobile-bed equilibrium allow a best fit of the measured elevation-specific entrainment rates E_{btt} in terms of the predicted values computed from $E_b\, p_{Ent}(y)\, \Delta y$, and thus permit determination of the corresponding total entrainment rate E_b for each equilibrium state. Figure 9 shows two examples of this fit; the upper panel corresponds to Run 3, for which the bedload transport rate was relatively low, while the lower panel corresponds to Run 1, for which the bedload transport rate was relatively high.

A power law correlation between the dimensionless entrainment rate $\hat{E}_b$:

$$\hat{E}_b = \frac{E_b}{\sqrt{RgD_{50}}} \tag{42}$$

and the (sidewall-corrected) Shields number τ^* yielded:

$$\hat{E}_b = 0.05\left(\tau^* - 0.0549\right)^{1.85} \tag{43}$$

The experimental data and entrainment predictor (43) are plotted in Figure 10. $\hat{E}_b$ accounts for any mobility factor corresponding to *Wilcock*'s [1997a] characterization of partial transport

because $\hat{E}_b$ quantifies the fraction of the bed area per unit time that is in transport. The method employed to estimate $\hat{E}_b$ precludes the potential mistake of confusing actual particle entrainment with net entrainment (i.e. entrainment minus deposition).

Let $\hat{L}_s$ denote the dimensionless step length, given as:

$$\hat{L}_s = \frac{L_s}{D_{50}} \tag{44}$$

Combining (3), (6), (9), and (42) to (44) yields the following predictor function in terms of the (sidewall-corrected) Shields number τ^*:

$$\hat{L}_s \cong 53.2\left(\tau^* - 0.0549\right)^{-0.35} \tag{45}$$

Equation (45) is contrary to the result of *Einstein* [1937], who deduced the step length L_s only depended on particle size diameter. As *Hassan et al.* [1991] point out, Einstein did not measure individual step lengths during his flume experiments. Instead, Einstein indirectly arrived at his conclusion by fitting a theoretical exponential probability model to the observed distribution of streamwise displacements of bed particles. According to (45), however, step length also depends weakly on excess shear stress. The form of (45) may be counterintuitive; the dimensionless step length $\hat{L}_s$ decreases weakly as the excess Shields number increases, varying between a high of 206 at low Shields number to a low of 139 at high Shields number for the range of experimental equilibrium states presented in this paper.

The decrease in step length with increasing Shields number has an important physical interpretation. To maintain mobile-bed equilibrium conditions, the entrainment and deposition rate must increase with increasing bedload transport rate; the probability that a moving bedload particle becomes trapped in the bed increases for larger values of the driving force. Equation (18)

supports this, since greater bed elevation fluctuations create a higher probability of low (bed elevation) points where bedload particles can become trapped. Thus for higher bedload transport rates, the ratio between the times when a particle is at rest and on the move is expected to be smaller [see e.g., *Habersack*, 2001; *McNamara and Borden*, 2004]. Additional support of this finding follows derivation of the predictor for particle virtual velocity below. Any increase in bedload transport rate is due to an increase in the entrainment rate and not an increase in step length, because the latter parameter decreases weakly with increasing Shields number.

5.4 Particle virtual velocity

Equation (25) was derived indirectly as a predictor of particle virtual velocity U_{pir} by combining equations (3), (7), (9), (17), (18), (23) and (24), based on measurements of the volume bedload transport rate and associated bed elevation fluctuations. A direct derivation of a predictor for U_{pir} is described below.

This approach is based on the hypothesis that, once travel distances are scaled with duration of competent flow (i.e., duration of experiment) then the resulting probability density function should be unique for a given equilibrium state. It could be argued that if the duration is very short the experimental data might be biased toward larger estimates of mean dimensionless particle virtual velocity $\hat{U}_{pir}$ because only the *first* (top) layer of tracer stones would be entrained and particle exchange would be limited relative to experiments of longer duration. Here this issue is addressed by evaluating an estimate for the mean value $\hat{U}_{pir}$ as well as a supportable approximation of the distribution of virtual velocities.

If run duration is sufficiently long numerous tracer stones are displaced beyond the limits of the flume and no precise information about travel distance can be obtained. This occurred

regularly during runs of 15-minute duration or longer, as illustrated by Figure 11. About 50% or more of displaced tracer stones for these durations belong to group *SD2*, i.e. those transported out of the flume. All that is known about the displacement distance of these particles is that it was longer than the distance from the seeding position to the downstream sediment trap at the end of the flume.

This problem can be approached by assuming a probability distribution for particle virtual velocities (an exponential or gamma distribution, as suggested from field experiments with tracer stones conducted by *Nakagawa and Tsujimoto*, 1980; *Hassan*, 1990; *Schmidt and Ergenzinger*, 1992; *Gintz et al.*, 1996; *Habersack*, 2001; *Ferguson et al.*, 2002; *Lenzi*, 2004; *McNamara and Borden*, 2004), then obtaining a mean value for travel distance from this probability distribution. To validate this assumption, the mean values of particle virtual velocity computed this way should statistically be about the same for all six run durations considered for each experimental equilibrium state.

Figure 12a shows a plot of the probability of non-exceedance P_{vir} (or cumulative distribution function) of particle virtual velocity $U_{pir-ith}$ as a function of test duration for Run 4. The six tests cover a wide range of durations, from 150 s (2.5 minutes) to 7200 s (2 hours), but all correspond to the same mobile-bed equilibrium. The cumulative distribution functions are essentially the same in all cases. A similar result is observed in Figure 12b corresponding to Run 2, in which experimental durations ranged from 90 s (1.5 minutes) to 7200 s (2 hours). The equilibrium state presented in Figure 12b corresponds to the second largest excess shear stress observed, whereas Figure 12a corresponds to the smallest. As a result, there is an observed shift to the right in the cumulative distribution function P_{vir}, corresponding to virtual velocities that increase with shear stress. This result indicates that whatever approach is followed to characterize particle virtual

velocity, it should include a measure of flow strength as one of the input parameters. Thus flow strength is characterized here in terms of the (sidewall-corrected) Shields number.

An estimate of the mean value of particle virtual velocity requires a priori information about travel distances corresponding to tracer stones in group *SD2*, i.e. those transported out of the flume. Data must be extrapolated beyond the range for which travel distances were observed and the associated uncertainty is larger for runs of longer duration. An alternative robust measure of central tendency, the median particle virtual velocity $U_{pir\text{-}50}$, however, can be computed without assuming the form of the probability distribution. Figure 12a and Figure 12b show the cumulative distribution function to be constant for a given mobile-bed equilibrium, and at least for runs *Short-1* and *Short-2* the value of $U_{pir\text{-}50}$ could be extracted. The dimensionless particle virtual velocity $\tilde{U}_{pir}$ is defined as:

$$\tilde{U}_{pir} = \frac{U_{pir-ith}}{U_{pir-50}} \tag{46}$$

When particle virtual velocities are scaled using (46), the cumulative distribution function $\tilde{P}_{vir}$ of $\tilde{U}_{pir}$ is independent of excess shear stress. Figure 13a is a plot of the empirical probability of non-exceedance of scaled virtual velocity $\tilde{P}_{vir}$ for the 10 experimental equilibrium states, including all runs corresponding to *Short-1*, i.e. runs of duration minimizing the number of tracer stones displaced out of the system. A narrow band depicted by two black thick dashed lines is included in this figure. This band encloses all empirical cumulative distribution functions, and its spread diminishes as $\tilde{U}_{pir}$ increases, with a cumulative probability spread less than 0.15 for values of $\tilde{U}_{pir}$ larger than unity. This is the first indication that the scaling of (46) results in a unique probability density function of particle virtual velocities.

Figure 13b shows results of similar analysis applied to runs corresponding to *Short-2*, i.e. twice the duration of *Short-1*. We note the band of Figure 13a encompasses nearly all of the *Short-2* experiment empirical cumulative distribution functions. The scaling proposed in (46) thus appears defendable, in this case for a range of values of $\tilde{U}_{pir}$ and their associated probability of non-exceedance $\tilde{P}_{vir}$ varying from minimum values of $\tilde{U}_{pir}$ of 0.22 and $\tilde{P}_{vir}$ of 8% to maximum values of $\tilde{U}_{pir}$ of 5.13 and $\tilde{P}_{vir}$ of 93%. The band is sufficiently narrow to allow approximation of a unique cumulative distribution function $\tilde{P}_{vir}\left(\tilde{U}_{pir}\right)$. Such a distribution must satisfy three constraints: (i) the probability of non-exceedance $\tilde{P}_{vir}$ should be 50% for $\tilde{U}_{pir}$ = 1; (ii) the curve should near the center of the narrow band; and (iii) $\tilde{P}_{vir}$ should approach unity as $\tilde{U}_{pir}$ approaches infinity. Results of tracer field studies [e.g., *Nakagawa and Tsujimoto*, 1980; *Hassan*, 1990; *Schmidt and Ergenzinger*, 1992; *Gintz et al.*, 1996; *Habersack*, 2001; *Ferguson et al.*, 2002; *Lenzi*, 2004; *McNamara and Borden*, 2004] motivate the selection of a two-parameter gamma density function whose general form is:

$$f\left(\tilde{U}_{pir}\right)=\frac{d\tilde{P}_{vir}}{d\tilde{U}_{pir}}=\frac{\tilde{U}_{pir}^{k-1}\lambda^{k}\,\mathrm{e}^{-\lambda\tilde{U}_{pir}}}{\Gamma\left(k\right)} \tag{47}$$

where k is the shape parameter; λ is the scale parameter; and Γ is the gamma function. Our experimental data were fitted to a gamma probability density function with parameters $k = 0.85$, and $\lambda = 0.55$, illustrated also in Figure 13a and Figure 13b. The mean value $\overline{\tilde{U}}_{pir}$ of the dimensionless particle virtual velocity for this probability density function is 1.54, so that in dimensioned parameters:

$$U_{pir}=1.54U_{pir-50} \tag{48}$$

where U_{pir} is the mean value of the dimensioned particle virtual velocity, as defined in (7).

A power law regression between the dimensionless particle virtual velocity $\hat{U}_{pir}$ defined in (24) and the (sidewall-corrected) Shields number τ^* yielded:

$$\hat{U}_{pir} = 1.67\left(\tau^* - 0.0549\right)^{0.90} \tag{49}$$

Experimental data and the particle virtual velocity predictor (49) are plotted in Figure 14. The exponent of 0.90 in (49) is nearly identical to the value 0.94 in (25). Setting the exponents equal and equating (25) and (49) yields:

$$\alpha\left(P_{sa}\right) = 0.515 \tag{50}$$

in which case the normal probability density function (12) yields the relation:

$$P_{sa} = 0.584 \tag{51}$$

A comparison of the two functions (25) and (49) indicates that up to the order-one coefficient $\alpha(P_{sa})$, two predictors of particle virtual velocity derived using different methods yield essentially the same result.

6. Discussion

A comprehensive set of 80 flume experiments with tracer stones was conducted under conditions of lower-regime plane-bed equilibrium bedload transport of uniform gravel. The selections of well-sorted gravel and plane-bed conditions (no bedforms) were made to simplify as much as possible the study of entrainment, transport and deposition of tracer stones. Relations connecting the vertical and streamwise displacement patterns of tracer stones, corresponding channel-averaged hydraulic parameters and associated bulk sediment transport rate were developed.

Experimental data were used to derive empirical predictors for the statistics of bed elevation fluctuations, particle entrainment rates, particle step lengths and particle virtual velocities. These predictors improve quantification of the stochastic processes of particle entrainment, streamwise displacement and deposition which characterize bedload transport, and hence understanding the mechanics underlying the morphodynamics of gravel-bed streams. Bedload particles sporadically but constantly interchange with the bed, thus it is of value to develop reliable estimates of not only the mean parameters characterizing bedload transport but also associated probability density functions.

Simultaneous measurements of instantaneous bed elevation at different streamwise locations in the flume were carried out with a sonar-transducer system. These datasets were used to demonstrate that a normal probability model provides an excellent fit of the empirical distribution of the bed elevation fluctuations at mobile-bed equilibrium, whose standard deviation scales with the excess bed shear stress, or specifically the dimensionless Shields number. This observation allowed quantification of the thickness of the active layer, i.e. the depth of bed deposit constantly reworked by entrainment and re-occupation of space by individual particles. The predictor developed here indicates the thickness of the active layer correlates with both the representative grain size of bed material and the (sidewall-corrected) Shields number. An increase in flow strength drives a faster exchange process and more intense vertical reworking of the bed deposit, even at macroscopic mobile-bed equilibrium for which uniform and steady transport conditions prevail.

Positive correlation between the thickness of the active layer and flow strength has been suggested in the past. Based on fieldwork in seven gravel-bed streams located in British Columbia, Canada, *Haschenburger* [1999] found that the exchange depth of the bed deposit

increases with flow strength (as measured in terms of the peak flow of the hydrograph). A similar conclusion was reached by *Lenzi* [2004] as a result of systematic experiments on displacement and transport of marked bed particles (passive and active tracers) during floods conducted at a field station located on the Rio Cordon, Italy. Results obtained by *Hassan* [1990] from extensive field campaigns in Nahal Hebron and Nahal Og, Israel with tracer stones and scour chains also indicated that, in general, mean burial depth increases with Shields number. Furthermore, *Haschenburger and Church* [1998] found that during bedload transport events in armored gravel-bed streams, the bed is active at a minimum depth of 0.4 D_{90}, which corresponds to a value of the same order of magnitude as the range reported here for the standard deviation of bed elevation fluctuations. *Nikora et al.* [2001, 2002] also found comparable results, with a spatial (rather than temporal) standard deviation of bed elevation fluctuations of about 0.5 D_{50} to 0.6 D_{50}.

Our results for the total entrainment rate of bed sediment per unit bed area as a function of (sidewall-corrected) Shields number are similar to those obtained by using the equivalent relation proposed by *Fernández-Luque and van Beek* [1976], which was determined from careful measurements of particle deposition. A positive correlation between total entrainment rate and Shields number was found by *Nakagawa and Tsujimoto* at about the same time [1976, 1980], from direct measurements of particle entrainment. Results are also consistent with field measurements and numerical simulations performed by *Hassan and Church* [1994], *Haschenburger* [1999], and *Haschenburger and Wilcock* [2003], all of whom indicate that the mean depth of scour and fill increases with magnitude of peak discharge. Moreover, *Wu and Chou* [2003] re-analyzed experimental data from other researchers and found that the total probability of entrainment obtained by adding what they termed the "rolling" and "lifting"

probabilities, increases with Shields number. *McEwan et al.* [2004] later used this assumption in a probabilistic numerical model of the evolution of bedload composition.

The layered installation of tracers adopted in our experiments permitted for the first time a direct measurement of elevation-specific entrainment rates. An exponential function which incorporates the effect of bed elevation fluctuations via the standard deviation of fluctuations provided a good fit to the data. The selection of an exponential function for the vertical variation in entrainment rate is in accordance with the trends observed by other researchers when measuring scour and fill depths in gravel-bed streams located in areas ranging from flashy floods to snowmelt-dominated transport events [*Shick et al.*, 1987a, 1987b; *Hassan*, 1990; *Hassan and Church*, 1994; *Haschenburger*, 1999]. These authors argue that particles buried at a shallow depth should have a higher probability of entrainment into bedload transport than deeply buried ones, so that the percent of particles moved during a given flood should decrease with increasing depth of burial. We confirmed this with our experiments.

The elevation-specific deposition function, although not measured here, is hypothesized to be of the same form as the elevation-specific entrainment function. This hypothesis is in part based on an argument used by *Schick et al.* [1987a]. The fact that at mobile-bed equilibrium the total entrainment and deposition rates must be equal led these authors to argue the following: "Starting with a tracer population which is entirely surficial, the number of particles on the surface and in the subsurface becomes quasi-constant at a level determinable from the burial and exposure rates, which, in turn, also control the number of events needed to achieve equilibrium exchange." In other words, a geomorphic equilibrium state is attained when the number of tracer stones that are exhumed per unit time at any given level becomes equal to the number being buried per unit time at the same level within the bed deposit.

The predictor function for particle step length was indirectly derived from measurements of bedload transport rate and total entrainment rates. According to this predictor, and contrary to the common assumption made since the work of *Einstein* [1937], the step length depended not only on an appropriately chosen representative grain size of the bed material, but also was correlated weakly and negatively with Shields number [*Schmidt and Ergenzinger*, 1992; *Wilcock*, 1997a; *Habersack*, 2001]. This tendency for step length to decrease with increasing Shields number can be explained in terms of the increase in bed elevation fluctuations with increasing Shields number. An increase in the intensity of bed elevation fluctuations creates a higher probability of existence of low points where bedload particles can be trapped. When restricted to the range of Shields numbers comparable to the one used in our experiments, Figure 11 of *Nakagawa and Tsujimoto* [1976] also shows a decreasing trend in step length with increasing flow strength. These authors explained the negative correlation in terms of momentum loss of moving particles due to collision with protruding bed particles and other neighboring moving particles. *Tsujimoto et al.* [1990] later conducted laboratory experiments with uniform sand and "flat bed conditions", and found that the step length was not constant; its mean value varied between 80 and 250 times the sand diameter, a range comparable to the range of mean values reported here for plane-bed transport of uniform gravel.

Our experiments with tracer stones allow determination of a predictor for the mean value of particle virtual velocity, again as a function of Shields number. This estimate is independent of the duration of competent flow, as previously hypothesized by *Wilcock* [1997b] for bedload transport under steady, uniform conditions. The mean values for particle virtual velocity obtained here are comparable, for instance, with those obtained by *Gintz et al.* [1996] from field measurements during five summers in the Lainbach River, Germany. The results of the work by

Lenzi [2004] also provide estimates of the same order of magnitude. Slightly smaller estimates were obtained by *Haschenburger and Church* [1998] in Carnation Creek, Canada. The only authors who find significantly lower values of the mean particle virtual velocity are *Ferguson et al.* [2002], based on 8 years of field measurements in Allt Dubhaig, Scotland. The measurements of virtual velocity of gravel of *Ferguson et al.* [2002] were, however, taken not far upstream of a gravel-sand transition.

7. Conclusions

The experiments reported here pertain to the entrainment, transport and deposition of gravel tracers of uniform size in a flume containing the same uniform material at mobile-bed equilibrium under plane-bed conditions. The experiments:

- justify a bedload transport equation of the general type of *Meyer-Peter and Müller* [1948], but with a lower coefficient;
- indicate that bed elevation fluctuations fit a normal distribution;
- yield a predictor for the standard deviation of bed elevation fluctuations as a function of grain size and Shields number;
- yield a predictor for active layer thickness that increases with both grain size and Shields number;
- show that a dimensionless measure of entrainment rate can also be related to the Shields number;
- illustrate that the elevation-specific probability density of entrainment decreases exponentially with depth below the mean bed surface;

- yield a predictor for particle step length that increases with grain size but weakly decreases with increasing Shields number;
- result in a predictor for particle virtual velocity that increases with grain size and Shields number; and finally,
- yield a universal dimensionless function for the probability distribution of particle virtual velocity that is independent of the duration of competent flow.

The above results are sufficient to specify most of the parameters in a probabilistically based numerical model of tracer entrainment, transport and deposition based on the framework of *Parker et al.* [2000] and modified by *Blom and Parker* [2004]. The implementation of such a model represents a challenge for the future.

Notation

D_b volume rate of deposition per unit bed area ($L\ T^{-1}$).

D_g geometric mean particle size (L).

D_{tr} volume deposition rate of tracers per unit bed area ($L\ T^{-1}$).

D_{50} median particle size (L).

D_{90} particle size for which 90% of the sediment is finer (L).

E_b volume rate of entrainment per unit bed area ($L\ T^{-1}$).

$\hat{E}_b$ dimensionless volume rate of entrainment per unit bed area (1).

E_{btt} layer-specific volume entrainment rate of sediment per unit bed area ($L\ T^{-1}$).

E_{tr} volume entrainment rate of tracers per unit bed area ($L\ T^{-1}$).

f_{bti} fraction remaining of the total number of tracer stones installed within the bed (1).

$f\left(\tilde{U}_{pir}\right)$ probability density function of dimensionless particle virtual velocities (1).

g acceleration of gravity (L T^{-2}).

H water depth (L).

k shape parameter of gamma probability density function (1).

L_a thickness of the active layer (L).

$\hat{L}_a$ dimensionless thickness of the active layer (1).

L_s particle step length (L).

$\hat{L}_s$ dimensionless particle step length (1).

N size of the dataset.

$p_B(y)$ appropriately chosen normalizing probability density function (L^{-1}).

$p_{Dep}(y)$ probability density function that a bedload particle is deposited onto the bed deposit at a depth y relative to the mean bed elevation η (L^{-1}).

$p_e(y)$ probability density function of bed elevation fluctuations (L^{-1}).

$p_{Ent}(y)$ probability density function that a particle entrained from the bed deposit into bedload transport comes from a depth y relative to the mean bed elevation η (L^{-1}).

$P_S(y)$ cumulative distribution function of bed elevation fluctuations (1).

P_{sa} cumulative distribution function of bed elevation fluctuations evaluated at $y = y_a$ (1).

P_{vir} cumulative distribution function of particle virtual velocities (1).

$\tilde{P}_{vir}$ cumulative distribution function of dimensionless particle virtual velocities (1).

q_b volume bedload transport per unit width of channel per unit time (L^2 T^{-1}).

Q_{bf} constant rate of sediment supply (M T^{-1}).

Q_w constant water discharge ($L^3\ T^{-1}$).

q^* dimensionless volume bedload transport per unit width of channel per unit time, or Einstein number (1).

R submerged specific gravity of the sediment (1).

s_y standard deviation of bed elevation fluctuations (L).

$\hat{s}_y$ dimensionless standard deviation of bed elevation fluctuations (1).

s_y^2 variance of bed elevation fluctuations (L^2).

S_w streamwise water surface slope (1).

S_0 streamwise bed surface slope (1).

t time (T).

U_{bm} particle bedload velocity ($L\ T^{-1}$).

U_{pir} particle virtual velocity ($L\ T^{-1}$).

$\hat{U}_{pir}$ dimensionless particle virtual velocity (1).

$\tilde{U}_{pir}$ dimensionless particle virtual velocity, scaled with respect to the median value $U_{pir\text{-}50}$ (1).

$\overline{\tilde{U}}_{pir}$ mean value of the dimensionless particle virtual velocity (1).

$U_{pir-ith}$ any given value of the particle virtual velocity ($L\ T^{-1}$).

$U_{pir\text{-}50}$ median particle virtual velocity ($L\ T^{-1}$).

y deviation from mean bed elevation (L).

$\overline{y}$ mean value of deviations from mean bed elevation (L).

y_a relative position in the bed at which the cumulative distribution function of bed elevation fluctuations attains a value close to unity (L).

y_{bE} offset distance from the mean bed elevation for the entrainment function (L).

y_{bD} offset distance from the mean bed elevation for the deposition function (L).

y_i ith value of the deviation y from the mean bed elevation η (L).

y_0 bias common to both the entrainment and the deposition functions (L).

y_1 offset distance biasing entrainment toward higher elevations than deposition (L).

z instantaneous bed elevation (L).

z_{tr} thickness of layer of tracer stones (L).

α scaling coefficient for thickness of active layer in terms of standard deviation of bed elevation fluctuations (1).

Γ gamma function.

η mean bed elevation (L).

λ scale parameter of gamma probability density function (1).

ρ density of water (M L^{-3}).

ρ_s density of sediment (M L^{-3}).

σ_g geometric standard deviation (1).

τ_b bed shear stress (M L^{-1} T^{-2}).

τ^* dimensionless bed shear stress, or Shields number (1).

τ^*_{cr} critical Shields number (1).

ξ_b volume of particles in beload motion per unit bed area (L).

Acknowledgments

This work was supported by the National Science Foundation via Agreement Numbers EAR-0207274 and EAR-0207272. Additional support was derived from the STC program of the

National Science Foundation via the National Center for Earth-surface Dynamics under Agreement Number EAR-0120914, the Sommerfeld Graduate Fellowship (first author) of the Department of Civil Engineering, University of Minnesota and The Edward Silberman Fellowship (first author) of the St. Anthony Falls Laboratory, University of Minnesota. This paper represents a contribution of the research of the National Center for Earth-surface Dynamics in the area of channel dynamics. Andrew Fyten, Danielle Trice, Robert Haydel, Andrew Nguyen and Adele Braun actively participated in the design and execution of the experimental runs. Carl Peterson and Jim Mullin worked on the algorithm for measuring the bed elevation fluctuations with the sonar-transducer system.

References

Armanini, A. (1995), Non-uniform sediment transport: dynamics of the active layer, *J. Hydraul. Res.*, *33*(5), 611-622.

Barry, J. J., J. M. Buffington, and J. G. King (2004), A general power equation for predicting bed load transport rates in gravel bed rivers, *Water Resour. Res.*, *40*(10), W10401, doi:10.1029/2004WR003190, 22 pp.

Blom, A. (2003), A vertical sorting model for rivers with non-uniform sediment and dunes, Ph.D. thesis, 267 pp., University of Twente, Twente, the Netherlands.

Blom, A., and G. Parker (2004), Vertical sorting and the morphodynamics of bed form-dominated rivers: A modeling framework, *J. Geophys. Res.*, *109*, F02007, doi:10.1029/2003JF000069, 15 pp.

Borah, D. K., C. V. Alonso, and S. N. Prasad (1982), Routing graded sediments in streams: Formulations, *J. Hydraul. Div. ASCE*, *108*(HY12), 1486-1503.

Bridge, J. S., and S. J. Bennett (1992), A model for the entrainment and transport of sediment grains of mixed sizes, shapes and densities, *Water Resour. Res.*, *28*(2), 337-363.

Bridge, J. S., and D. F. Dominic (1984), Bed load grain velocities and sediment transport rates, *Water Resour. Res.*, *20*(4), 476-490.

Buffington, J. M., and D. R. Montgomery (1999), Effects of hydraulic roughness on surface textures of gravel-bed rivers, *Water Resour. Res.*, *35*(11), 3507-3521.

Cao, Z., and P. A. Carling (2002), Mathematical modeling of alluvial rivers: reality and myth. Part 1: General review, *Water Maritime Engng.*, *154*(3), 207-219.

Carling, P. A., and N. Wood (1994), Simulation of flow over pool-riffle topography: A consideration of the velocity reversal hypothesis, *Earth Surf. Processes Landforms*, *19*(4), 319-332.

Church, M., and M. A. Hassan (1992), Size and distance of travel of unconstrained clasts on a streambed, *Water Resour. Res.*, *28*(1), 299-303.

Crickmore, M. J., and G. H. Lean (1962a), The measurement of sand transport by means of radioactive tracers, *Proc. R. Soc. Lond.*, *A 266*(1326), 402-421.

Crickmore, M. J., and G. H. Lean (1962b), The measurement of sand transport by the time-integration method with radioactive tracers, *Proc. R. Soc. Lond.*, *A 270*(1340), 27-47.

DeVries, P. (2000), Scour in low gradient gravel bed streams: Patterns, processes, and implications for the survival of salmonid embryos, Ph.D. thesis, 365 pp., University of Washington, Seattle, Washington.

DeVries, P. (2002), Bedload layer thickness and disturbance depth in gravel bed streams, *J. Hydraul. Engng.*, *128*(11), 983-991.

Einstein, H. A. (1937), Der Geschiebetrieb als Wahrscheinlichkeitsproblem, in *Mitteilung der Versuchsanstalt für Wasserbau an der Eidgenössische Technische Hochschule Zürich*, Verlag Rascher, Zurich, Switzerland. (English translation, *Sedimentation*, edited by H. W. Shen, pp. C1-C105, Fort Collins, Colorado.)

Einstein, H. A. (1950), The bed-load function for sediment transportation in open channel flows, *Tech. Bull. 1026*, 78 pp., U. S. Department of Agriculture, Soil Conservation Service, Washington, D. C.

Ferguson, R. I., and S. J. Wathen (1998), Tracer-pebble movement along a concave river profile: Virtual velocity in relation to grain size and shear stress, *Water Resour. Res.*, *34*(8), 2031-2038.

Ferguson, R. I., D. J. Bloomer, T. B. Hoey, and A. Werritty (2002), Mobility of river tracer pebbles over different timescales, *Water Resour. Res.*, *38*(5), doi:10.1029/2001WR000254, 9 pp.

Fernández Luque, R., and R. van Beek (1976), Erosion and transport of bed-load sediment, *J. Hydraul. Res.*, *14*(2), 127-144.

Gintz, D., M. A. Hassan, and K. H. Schmidt (1996), Frequency and magnitude of bedload transport in a mountain river, *Earth Surf. Processes Landforms*, *21*(5), 433-445.

Gómez, B., and M. Church, (1989), An assessment of bedload sediment transport formulae for gravel bed rivers, *Water Resour. Res.*, *25*(6), 1161-1186.

Habersack, H. M. (2001), Radio-tracking gravel particles in a large braided river in New Zealand: a field test of the stochastic theory of bed load transport proposed by Einstein, *Hydrol. Processes*, *15*(3), 377-391.

Haschenburger, J. K. (1999), A probability model of scour and fill depths in gravel-bed channels, *Water Resour. Res.*, *35*(9), 2857-2869.

Haschenburger, J. K., and M. Church (1998), Bed material transport estimated from the virtual velocity of sediment, *Earth Surf. Processes Landforms*, *23*(9), 791-808.

Haschenburger, J. K., and P. R. Wilcock (2003), Partial transport in a natural gravel bed channel, *Water Resour. Res.*, *39*(1), 1020, doi:10.1029/2002WR001532, 9 pp.

Hassan, M. A. (1990), Scour, fill and burial depth of coarse material in gravel bed streams, *Earth Surf. Processes Landforms*, *15*(4), 341-356.

Hassan, M. A., and M. Church (1994), Vertical mixing of coarse particles in gravel bed rivers: A kinematic model, *Water Resour. Res.*, *30*(4), 1173-1186.

Hassan, M. A., and M. Church (2000), Experiments on surface structure and partial sediment transport on a gravel bed, *Water Resour. Res.*, *36*(7), 1885-1895.

Hassan, M. A., and P. Ergenzinger (2002), Use of tracers in fluvial geomorphology, in *Tools in fluvial geomorphology*, edited by G. M. Kondolf and H. Piégay, pp. 397-423, John Wiley and Sons, Hoboken, New Jersey.

Hassan, M. A., M. Church, and P. J. Ashworth (1992), Virtual rate and mean distance of travel of individual clasts in gravel-bed channels, *Earth Surf. Processes Landforms*, *17*(6), 617-627.

Hassan, M. A., M. Church, and A. P. Schick (1991), Distance of movement of coarse particles in gravel bed streams, *Water Resour. Res.*, *27*(4), 503-511.

Heald, J., I. McEwan, and S. Tait (2004), Sediment transport over a flat bed in a unidirectional flow: simulations and validation, *Phil. Trans. R. Soc. Lond.*, *A 362*(1822), 1973-1986.

Hirano, M. (1971), On riverbed variation with armoring, *Proc. Jpn. Soc. Civ. Eng.*, *195*, 55-65.

Hubbell, D. W., and W. W. Sayre (1964), Sand transport studies with radioactive tracers, *J. Hydraul. Div. ASCE*, *90*(HY3), 39-68.

Keller, E. A., and J. L. Florsheim (1993), Velocity-reversal hypothesis: A model approach, *Earth Surf. Processes Landforms*, *18*(8), 733-740.

Kuhnle, R. A. (1992), Bed load transport during rising and falling stages on two small streams, *Earth Surf. Processes Landforms*, *17*(2), 191-197.

Lenzi, M. A. (2004), Displacement and transport of marked pebbles, cobbles and boulders during floods in a steep mountain stream, *Hydrological Processes*, *18*(10), 1899-1914.

Lisle, T. E., F. ISEYA, and H. IKEDA (1993), Response of a channel with alternate bars to a decrease in supply of mixed-size bed load: A flume experiment, *Water Resour. Res.*, *29*(11), 3623-3629.

Lisle, T. E., J. M. Nelson, J. Pitlick, M. A. Madej, and B. L. Barkett (2000), Variability of bed mobility in natural, gravel-bed channels and adjustments to sediment load at local and reach scales, *Water Resour. Res.*, *36*(12), 3743-3755.

Malmaeus, J. M., and M. A. Hassan (2002), Simulation of individual particle movement in a gravel streambed, *Earth Surf. Processes Landforms*, *27*(1), 81-97.

Marion, A., S. J. Tait, and I. K. McEwan (2003), Analysis of small-scale gravel bed topography during armoring, *Water Resour. Res.*, *39*(12), 1334, doi:10.1029/2003WR002367, 11 pp.

McEwan, I., M. Sørensen, J. Heald, S. Tait, G. Cunningham, D. Goring, and B. Willets (2004), Probabilistic modeling of bed-load composition, *J. Hydraul. Engng.*, *130*(2), 129-139.

McNamara, J. P., and C. Borden (2004), Observations on the movement of coarse gravel using implanted motion-sensing radio transmitters, *Hydrol. Processes*, *18*(10), 1871-1884.

Meyer-Peter, E., and R. Müller (1948), Formulas for bed-load transport, in *Proceedings of the 2nd IAHR Meeting*, IAHR, pp. 39-64, Stockholm, Sweden.

Misri, R. L., R. J. Garde, and K. G. Ranga Raju (1984), Bed load transport of coarse nonuniform sediment, *J. Hydraul. Engng.*, *110*(3), 312-328.

Nakagawa, H., and I. Nezu (1977), Prediction of the contributions to the Reynolds stress from bursting events in open-channel flows, *J. Fluid Mech.*, *80*(1), 99-128.

Nakagawa, H., and T. Tsujimoto (1976), On probabilistic characteristics of motion of individual sediment particles on stream beds, in *Proceedings of the 2nd IAHR International Symposium on Stochastic Hydraulics*, IAHR, pp. 293-316, Lund, Sweden.

Nakagawa, H., and T. Tsujimoto (1980), Sand bed instability due to bed load motion, *J. Hydraul. Div. ASCE*, *106*(HY12), 2029-2051.

Nelson, J. M., J. P. Bennett, and S. M. Wiele (2002), Flow and sediment-transport modeling, in *Tools in fluvial geomorphology*, edited by G. M. Kondolf and H. Piégay, pp. 539-576, John Wiley and Sons, Hoboken, New Jersey.

Nikora, V., J. Heald, D. Goring, and I. McEwan (2001), Diffusion of saltating particles in unidirectional water flow over a rough granular bed, *J. Phys. A: Math. Gen.*, *34*(50), L743-L749.

Nikora, V., H. Habersack, T. Huber, and I. McEwan (2002), On bed particle diffusion in gravel bed flows under weak bed load transport, *Water Resour. Res.*, *38*(6), 1081, doi:10.1029/ 2001WR000513, 9 pp.

Niño, Y., and M. García (1994), Gravel saltation: 2. Modeling, *Water Resour. Res.*, *30*(6), 1915-1924.

Niño, Y., M. García, and L. Ayala (1994), Gravel saltation: 1. Experiments, *Water Resour. Res.*, *30*(6), 1907-1914.

Paintal, A. S. (1971), A stochastic model of bed load transport, *J. Hydraul. Res.*, *9*(4), 527-554.

Papanicolaou, A. N., P. Diplas, N. Evaggelopoulos, and S. Fotopoulos (2002), Stochastic incipient motion criterion for spheres under various bed packing conditions, *J. Hydraul. Engng.*, *128*(4), 369-380.

Parker, G. (1990), Surface-based bedload transport relation for gravel rivers, *J. Hydraul. Res.*, *28*(4), 417-436.

Parker, G., C. Paola, and S. Leclair (2000), Probabilistic Exner sediment continuity equation for mixtures with no active layer, *J. Hydraul. Engng.*, *126*(11), 818-826.

Pender, G., T. B. Hoey, C. Fuller, and I. K. McEwan (2001), Selective bedload transport during the degradation of a well sorted graded sediment bed, *J. Hydraul. Res.*, *39*(3), 269-277.

Pyrce, R. S., and P. E. Ashmore (2003), The relation between particle length distributions and channel morphology in gravel-bed streams: a synthesis, *Geomorphology*, *56*(1-2), 167-187.

Pyrce, R. S., and P. E. Ashmore (2005), Bedload path length and point bar development in gravel-bed river models, *Sedimentology*, *52*(4), 167-187.

Ribberink, J.S. (1987), Mathematical modeling of one-dimensional morphological changes in rivers with non-uniform sediment, Ph.D. thesis, 200 pp., Delft University of Technology, Delft, the Netherlands.

Roy, A. G., T. Buffin-Bélanger, and S. Deland (1996), Scales of turbulent coherent flow structures in a gravel-bed river, in *Coherent flow structures in open channels*, edited by P. J. Ashworth, S. J. Bennett, J. L. Best, and S. J. McLelland, pp. 147-164, John Wiley & Sons Ltd., New York.

Schick, A. P., M. A. Hassan, and J. Lekach (1987a), A vertical exchange model for coarse bedload movement: Numerical considerations, in *Geomorphological models – Theoretical and empirical aspects*, edited by F. Ahnert, pp. 73-83, Catena Verlag, Cremlingen-Destedt.

Schick, A. P., J. Lekach, and M. A. Hassan (1987b), Bed load transport in desert floods: Observations in the Negev, in *Sediment transport in gravel-bed rivers*, edited by C. R. Thorne, J. C. Bathurst, and R. D. Hey, pp. 617-636, John Wiley & Sons Ltd., New York.

Schmeeckle, M. W., and J. M. Nelson (2003), Direct numerical simulation of bedload transport using a local, dynamic boundary condition, *Sedimentology*, *50*(2), 279-301.

Schmidt, K. H., and P. Ergenzinger (1992), Bedload entrainment, travel lengths, step lengths, rest periods – studied with passive (iron, magnetic) and active (radio) tracer techniques, *Earth Surf. Processes Landforms*, *17*(2), 147-165.

Sear, D. A. (1996), Sediment transport processes in pool-riffle sequences, *Earth Surf. Processes Landforms*, *21*(3), 241-262.

Sear, D. A., M. W. E. Lee, R. J. Oakey, P. A. Carling, and M. B. Collins (2000), Coarse sediment tracing technology in littoral and fluvial environments: A review, in *Tracers in geomorphology*, edited by I. D. L. Foster, pp. 21-55, John Wiley & Sons Ltd., Chichester, UK.

Sekine, M., and H. Kikkawa (1992), Mechanics of saltating grains. II, *J. Hydraul. Engng.*, *118*(4), 536-558.

Shvidchenko, A. B., and G. Pender (2000), Initial motion of streambeds composed of coarse uniform sediments, *Water Maritime Engng.*, *142*(4), 217-227.

Sun, Z., and J. Donahue (2000), Statistically derived bedload formula for any fraction of nonuniform sediment, *J. Hydraul. Engng.*, *126*(2), 105-111.

Tsujimoto, T. (1990), Instability of longitudinal distribution of fluvial bed-surface composition, *J. Hydroscience Hydraul. Engng.*, *7*(2), 69-80.

Tsujimoto, T., and K. Motohashi (1990), Static armoring and dynamic pavement, *J. Hydroscience Hydraul. Engng.*, *8*(1), 55-67.

Tsujimoto, T., A. Mori, T. Okabe, and T. Ohmoto (1990), Non-equilibrium sediment transport: A generalized model, *J. Hydroscience Hydraul. Engng.*, *7*(2), 1-25.

Vanoni, V. A. (Ed.) (1975), *Sedimentation engineering - ASCE Manuals and Reports on Engineering Practice No. 54*, 745 pp., ASCE, New York.

Wiberg, P. L., and J. D. Smith (1989), Model for calculating bed load transport of sediment, *J. Hydraul. Engng.*, *115*(1), 101-123.

Wilcock, P. R. (1997a), The components of fractional transport rate, *Water Resour. Res.*, *33*(1), 247-258.

Wilcock, P. R. (1997b), Entrainment, displacement, and transport of tracer gravels, *Earth Surf. Processes Landforms*, *22*(12), 1125-1138.

Wilcock, P. R. (2004), Sediment transport in the restoration of gravel-bed rivers, in *Proceedings EWRI Congress 2004*, ASCE, 11 pp., Salt Lake City, Utah.

Wilcock, P.R., and J. C. Crowe (2003), Surface-based transport model for mixed-size sediment, *J. Hydraul. Engng.*, *129*(2), 120-128.

Wu, F. C., and Y. J. Chou (2003), Rolling and lifting probabilities for sediment entrainment, *J. Hydraul. Engng.*, *129*(2), 110-119.

Wu, F. C., and K. H. Yang (2004), A stochastic partial transport model for mixed-size sediment: Application to assessment of fractional mobility, *Water Resour. Res.*, *40*, W04501, doi:10.1029/2003WR002256, 18 pp.

Yalin, M. S., and H. Scheuerlein (1988), Friction factors in alluvial rivers, *59*, Institut für Wasserbau und Wassermengenwirtschaft und Versuchsanstalt für Wasserbau Oskar v. Miller in Obernach, Technische Universität München, Munich, Germany.

Yang, C. T., and C. Huang (2001), Applicability of sediment transport formulas, *Int. J. Sed. Res.*, *16*(3), 335-353.

Figure captions

Figure 1 Sample survey of streamwise profiles of the water and bed surfaces after lower-regime plane-bed equilibrium conditions had been attained in Run 9.

Figure 2 Time series of bed elevation measurements with ultrasonic transducer probes. Simultaneous recording at five different streamwise positions along the flume (see legend). (a) Run 10; (b) Run 8.

Figure 3 Fraction of tracers moved as a function of: (i) duration of experiment (horizontal axis), and (ii) initial depth of burial (see legend: the *first* layer was flush with the bed surface, and the *fourth* layer was buried the deepest). (a) Run 9; (b) Run 2.

Figure 4 Mean travel distance scaled by test duration for shortest test durations (Runs 4 and 11) for tracer stones in groups *SD3* and *SD4*. The data are further divided into four sub-groups, which indicate the initial and final position of the tracers; "surf" denotes bed surface, and "bur" denotes buried within the bed.

Figure 5 Bedload transport relation derived from experiments at SAFL. The database included both runs with tracer stones and runs without painted particles.

Figure 6 Empirical and theoretical normal cumulative distribution function of bed elevation fluctuations. (a) Run 10; (b) Run 8.

Figure 7 Sketch of temporal bed elevation fluctuations around mean bed elevation at a given streamwise location. Horizontal axis depicts time.

Figure 8 Fraction of tracers moved as a function of: (i) excess Shields number (horizontal axis), and (ii) initial depth of burial (see legend: the *first* layer was flush with the bed surface, and the *fourth* layer was buried the deepest). Flow duration: (a) 15 minutes; (b) 120 minutes.

Figure 9 Measured and predicted values of the dimensionless volume rate of entrainment per unit bed area as a function of particle burial depth with respect to mean bed elevation. (a) Run 3; (b) Run 1.

Figure 10 Measured and predicted values of the dimensionless volume rate of entrainment per unit bed area as a function of excess Shields number.

Figure 11 Fraction of displaced tracers in group *SD2* as a function of: (i) excess Shields number (horizontal axis), and (ii) duration of the experiment (see legend). Group *SD2* correspond to the painted particles that moved completely out of the system. The referred fraction is computed with respect to the total number of displaced tracers, not with respect to the total number of seeded tracers.

Figure 12 Cumulative distribution function of particle virtual velocities as a function of duration of the experiment (see legend). (a) Run 4; (b) Run 2.

Figure 13 Cumulative distribution function of dimensionless particle virtual velocities as a function of excess Shields number. The scaling of particle virtual velocities is with respect to the corresponding measured median value. Experiment duration: (a) *Short-1*; (b) *Short-2*. See the text for explanation about the thick black dashed and continuous lines.

Figure 14 Measured and predicted values of the dimensionless particle virtual velocity as a function of excess Shields number.

Table 1: Run durations of experiments with tracer stones, which were designed to maximize the number of displaced painted particles which moved within the limits of the flume.

Run	Run duration (s)	
	Short-1	*Short-2*
1	90	180
2	90	180
3	135	270
4	150	300
5	110	220
7	135	270
8	110	220
9	180	360
10	150	300
11	90	180

Table 2: Experimental conditions for lower-regime plane-bed normal flow equilibrium bedload transport. Notation includes: Q_w, water discharge; Q_{bf}, sediment feed rate; S_0, streamwise bed surface slope; S_w, streamwise water surface slope; and H, water depth.

Run	Q_w ($m^3\ s^{-1}$)	Q_{bf} ($kg\ s^{-1}$)	S_0 (%)	S_w (%)	H (m)
1	0.081	0.117	1.05	1.03	0.126
2	0.067	0.124	1.20	1.19	0.108
3	0.044	0.058	1.26	1.26	0.085
4	0.038	0.034	1.23	1.23	0.073
5	0.039	0.076	1.52	1.52	0.071
7	0.069	0.060	0.91	0.91	0.124
8	0.102	0.096	0.86	0.83	0.157
9	0.034	0.026	1.26	1.26	0.071
10	0.074	0.051	0.81	0.80	0.131
11	0.093	0.150	1.08	1.07	0.139

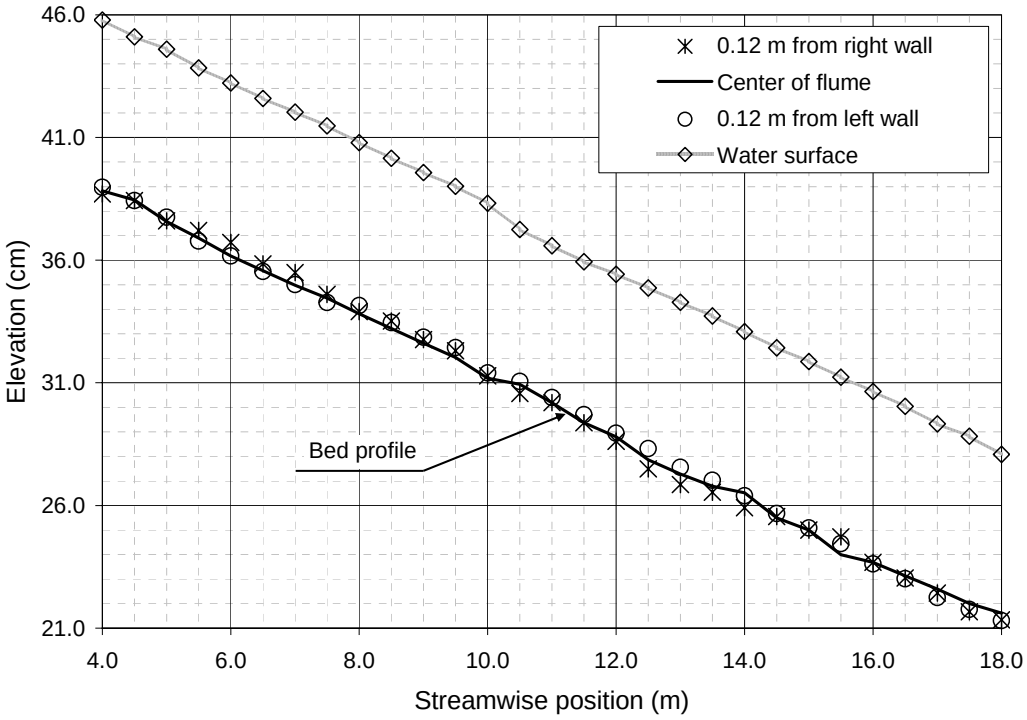
46.0
41.0
36.0
31.0
26.0
21.0
Elevation (cm)
4.0
6.0
8.0
10.0
12.0
14.0
16.0
18.0
Streamwise position (m)
0.12 m from right wall
Center of flume
0.12 m from left wall
Water surface
Bed profile

Figure 1

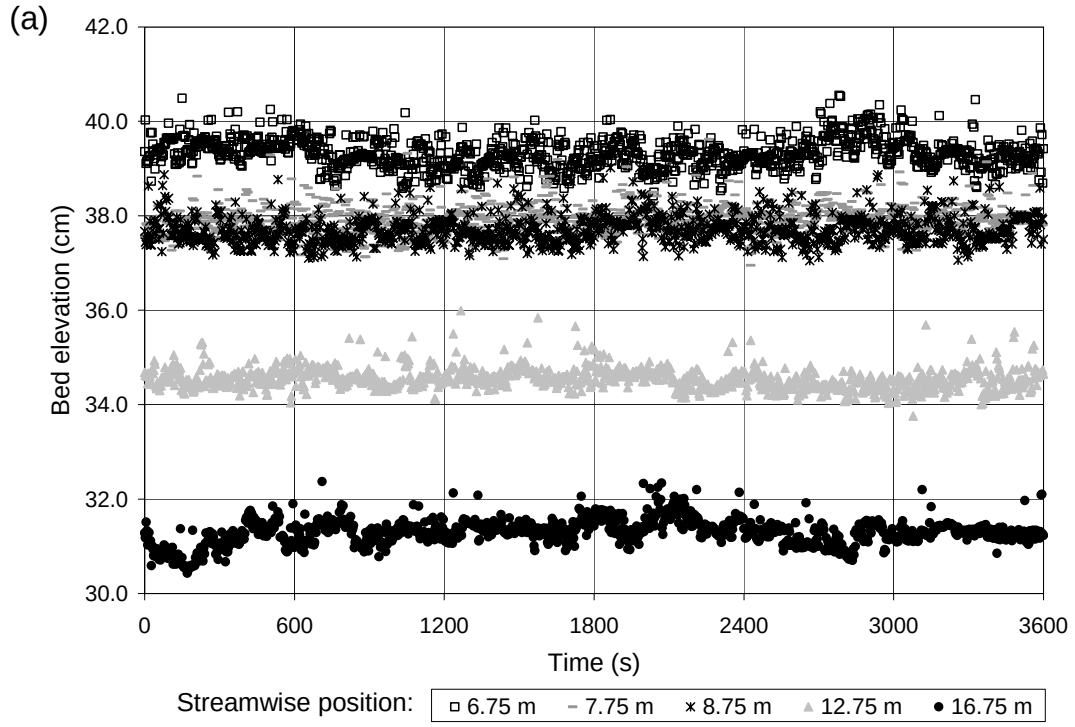
(a)
42.0
40.0
38.0
36.0
34.0
32.0
30.0
Bed elevation (cm)
0
600
1200
1800
2400
3000
3600
Time (s)
Streamwise position:
6.75 m
7.75 m
8.75 m
12.75 m
16.75 m

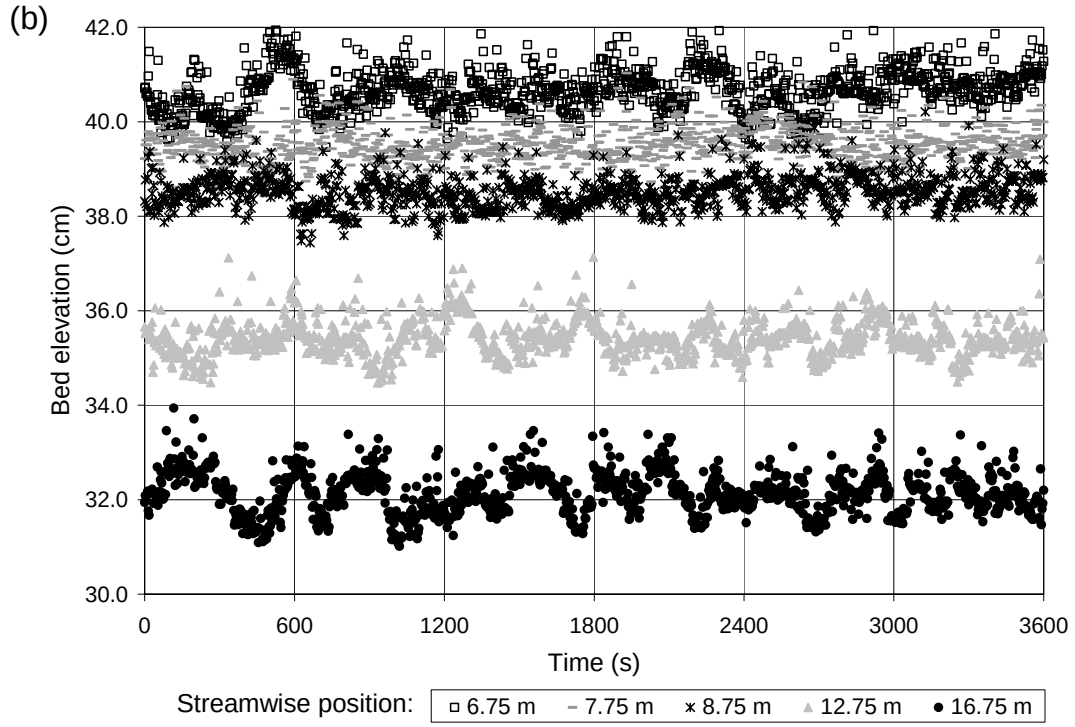
(b)
42.0
40.0
38.0
36.0
34.0
32.0
30.0
Bed elevation (cm)
0
600
1200
1800
2400
3000
3600
Time (s)
Streamwise position:
6.75 m
7.75 m
8.75 m
12.75 m
16.75 m

Figure 2

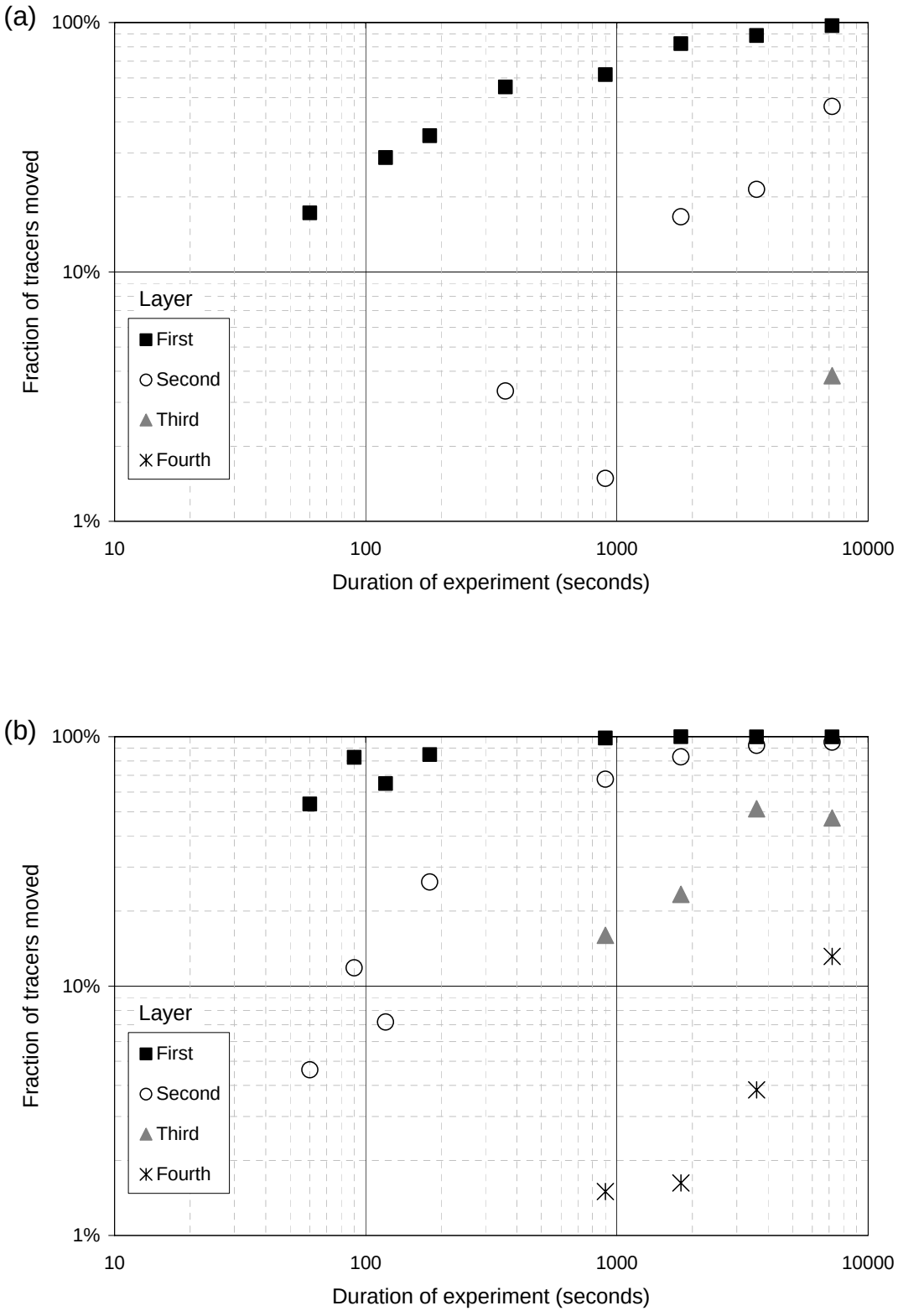
(a)
100%
10%
1%
Fraction of tracers moved
Layer
First
Second
Third
Fourth
10
100
1000
10000
Duration of experiment (seconds)
(b)
100%
10%
1%
Fraction of tracers moved
Layer
First
Second
Third
Fourth
10
100
1000
10000
Duration of experiment (seconds)

Figure 3

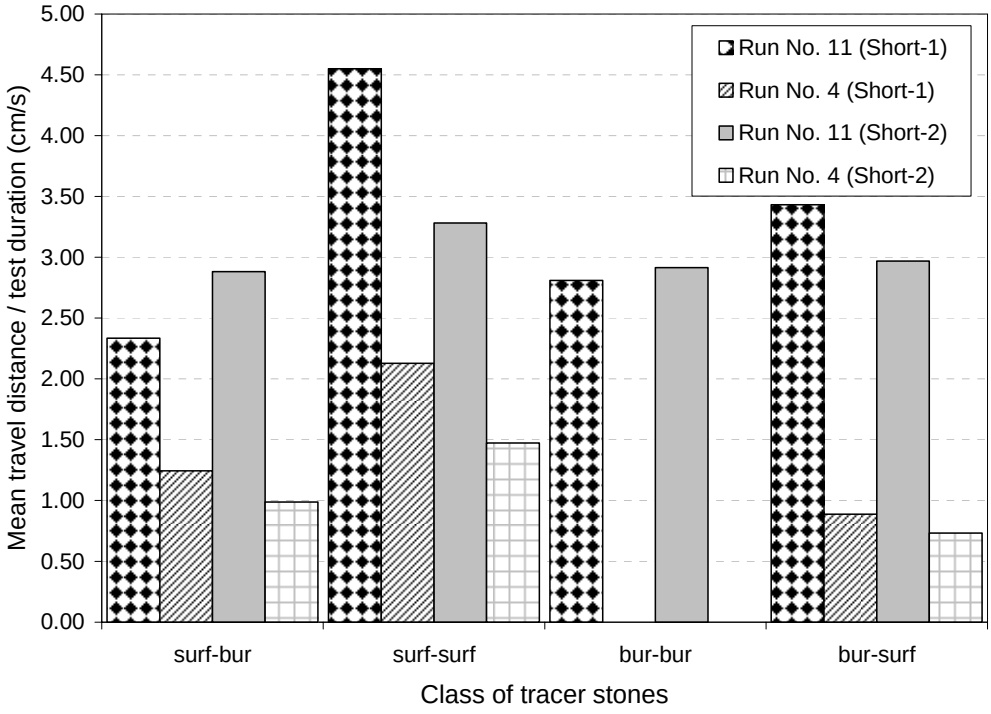
5.00
4.50
4.00
3.50
3.00
2.50
2.00
1.50
1.00
0.50
0.00
Mean travel distance / test duration (cm/s)
Run No. 11 (Short-1)
Run No. 4 (Short-1)
Run No. 11 (Short-2)
Run No. 4 (Short-2)
surf-bur
surf-surf
bur-bur
bur-surf
Class of tracer stones

Figure 4

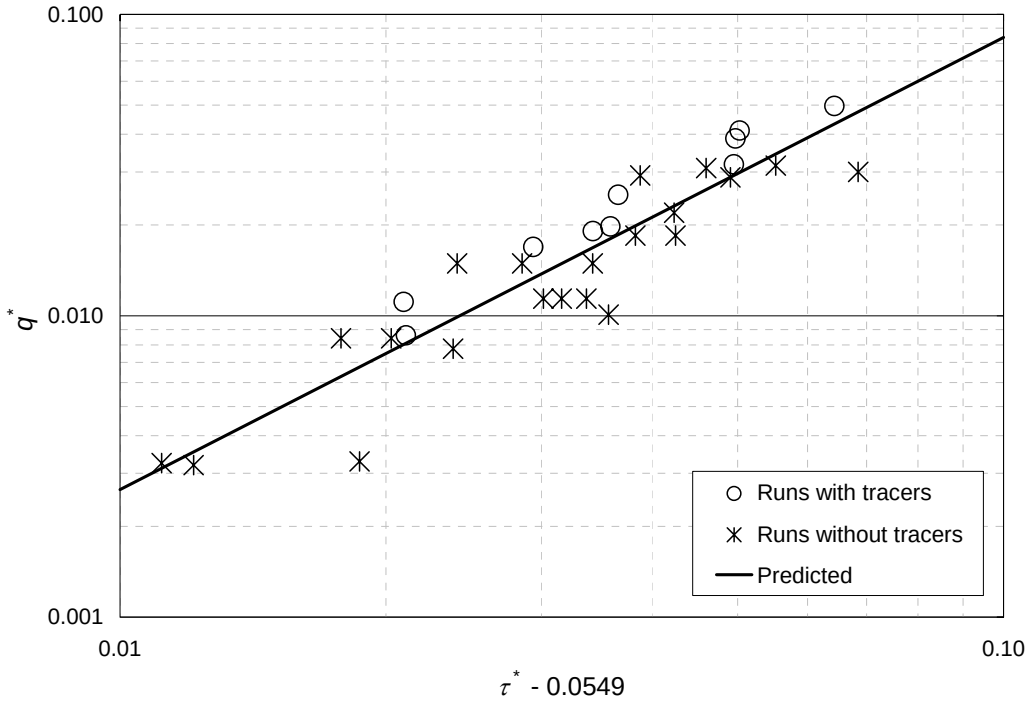
0.100
0.010
0.001
q^*
0.01
0.10
τ^* - 0.0549
Runs with tracers
Runs without tracers
Predicted

Figure 5

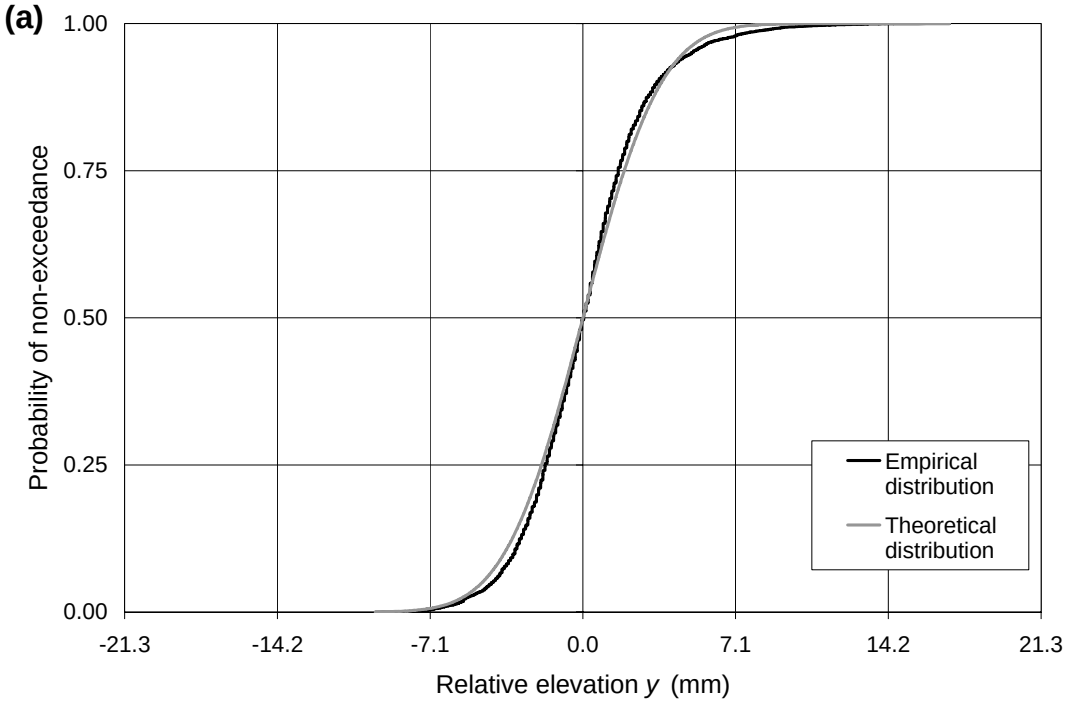
(a)
1.00
0.75
0.50
0.25
0.00
Probability of non-exceedance
-21.3
-14.2
-7.1
0.0
7.1
14.2
21.3
Relative elevation y (mm)
Empirical distribution
Theoretical distribution

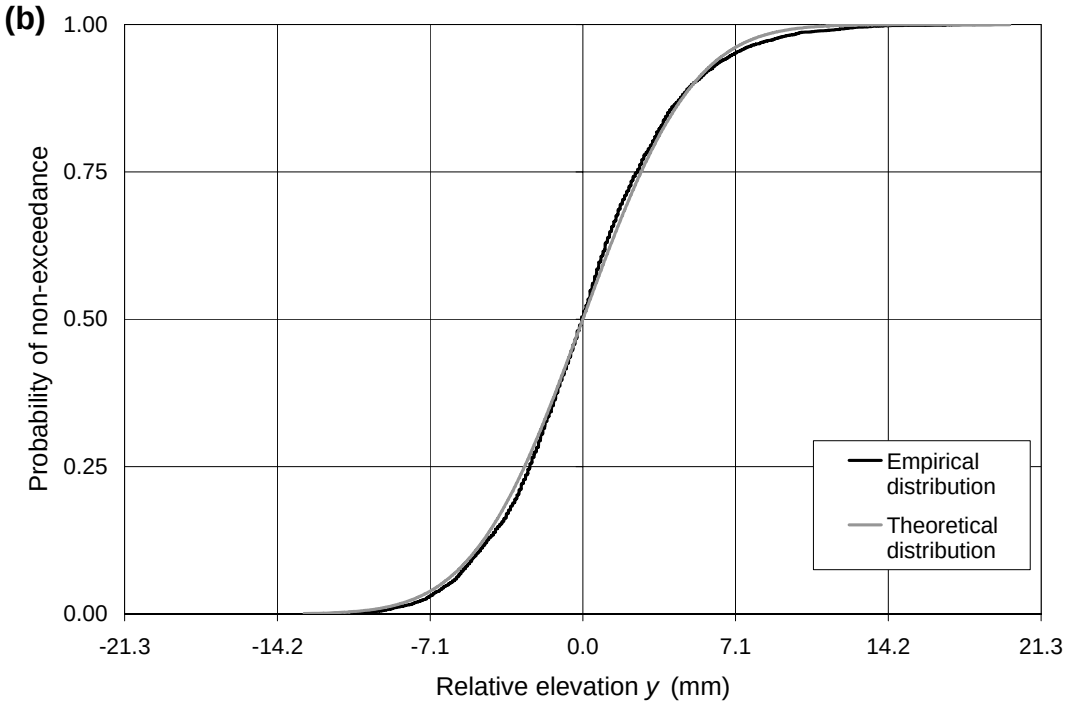
(b)
1.00
0.75
0.50
0.25
0.00
Probability of non-exceedance
-21.3
-14.2
-7.1
0.0
7.1
14.2
21.3
Relative elevation y (mm)
Empirical distribution
Theoretical distribution

Figure 6

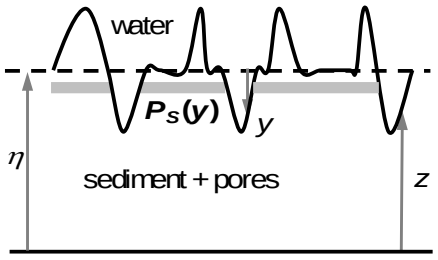

Figure 7

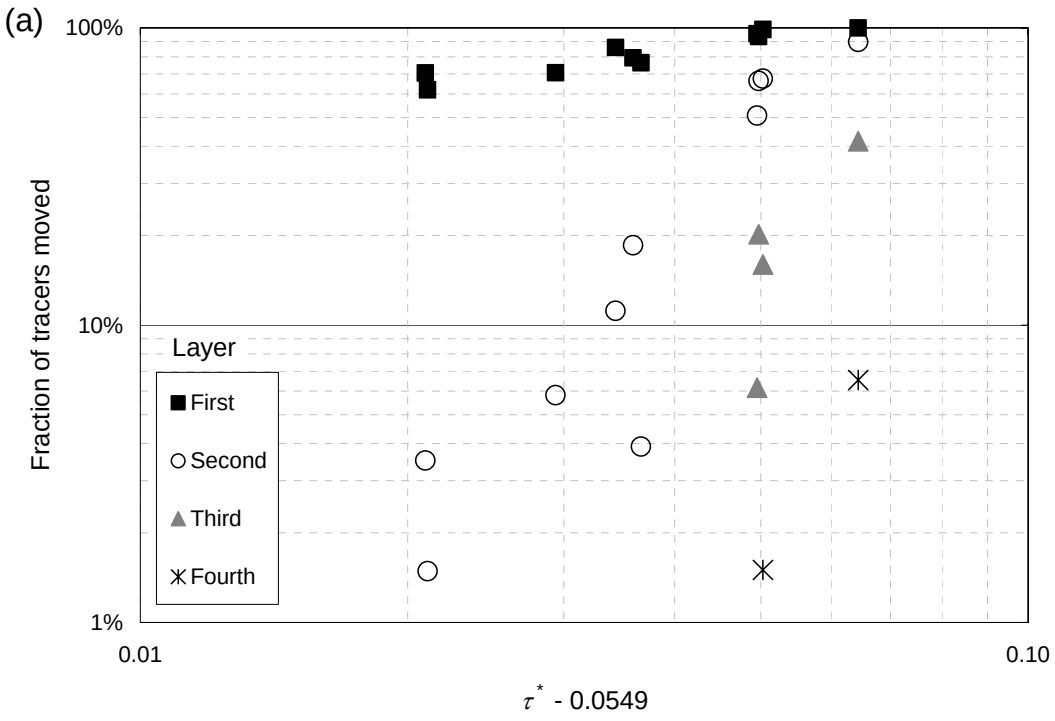
(a)
100%
10%
1%
Fraction of tracers moved
Layer
First
Second
Third
Fourth
0.01
0.10
τ^* - 0.0549

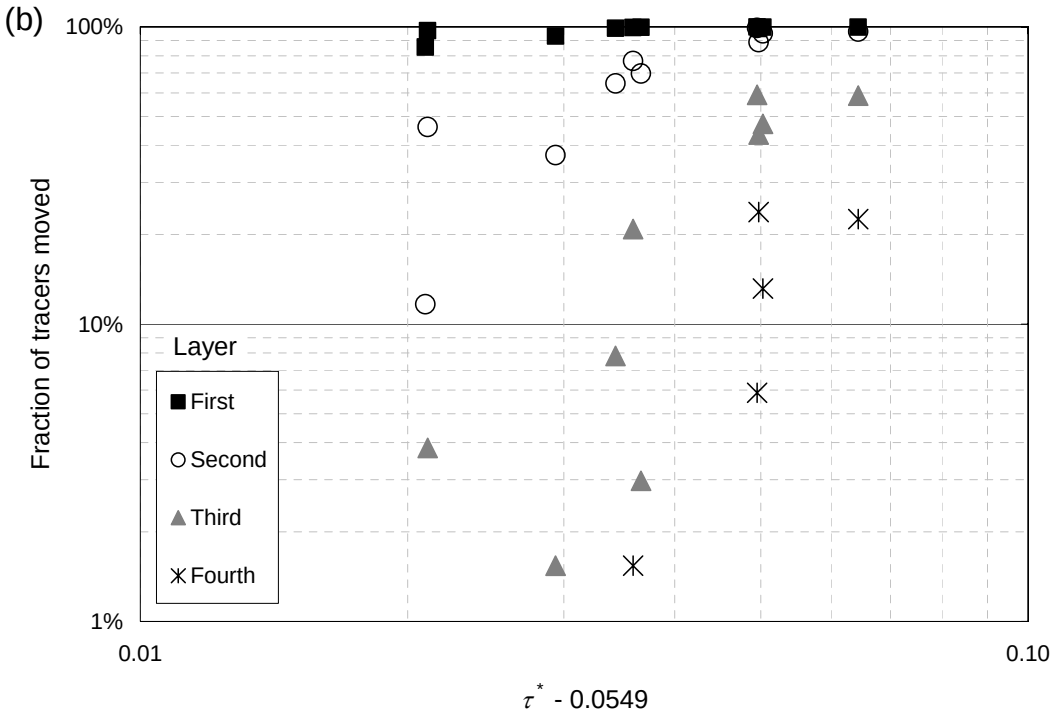
(b)
100%
10%
1%
Fraction of tracers moved
Layer
First
Second
Third
Fourth
0.01
0.10
τ^* - 0.0549

Figure 8

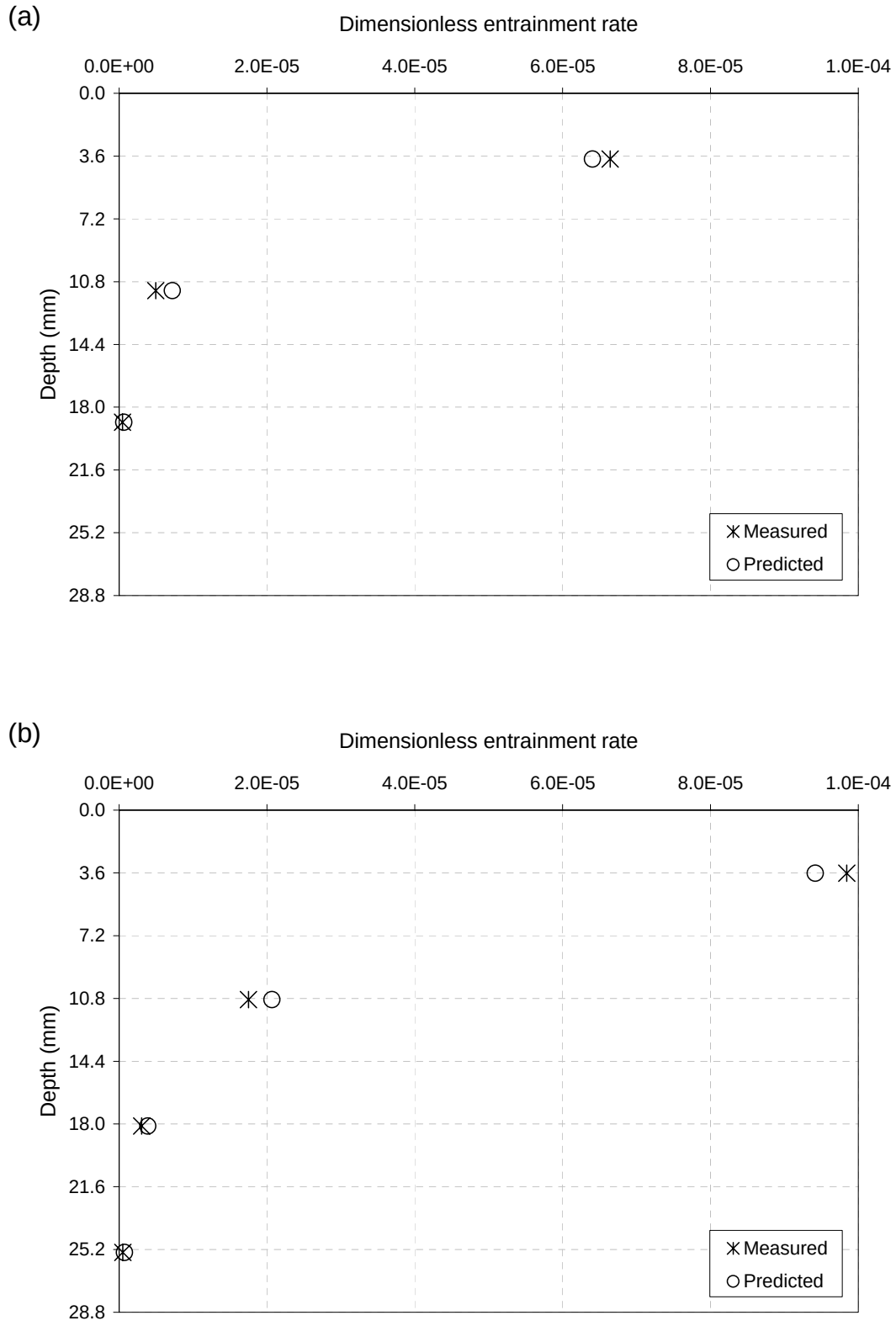
(a)
Dimensionless entrainment rate
0.0E+00
2.0E-05
4.0E-05
6.0E-05
8.0E-05
1.0E-04
0.0
3.6
7.2
10.8
14.4
18.0
21.6
25.2
28.8
Depth (mm)
Measured
Predicted
(b)
Dimensionless entrainment rate
0.0E+00
2.0E-05
4.0E-05
6.0E-05
8.0E-05
1.0E-04
0.0
3.6
7.2
10.8
14.4
18.0
21.6
25.2
28.8
Depth (mm)
Measured
Predicted

Figure 9

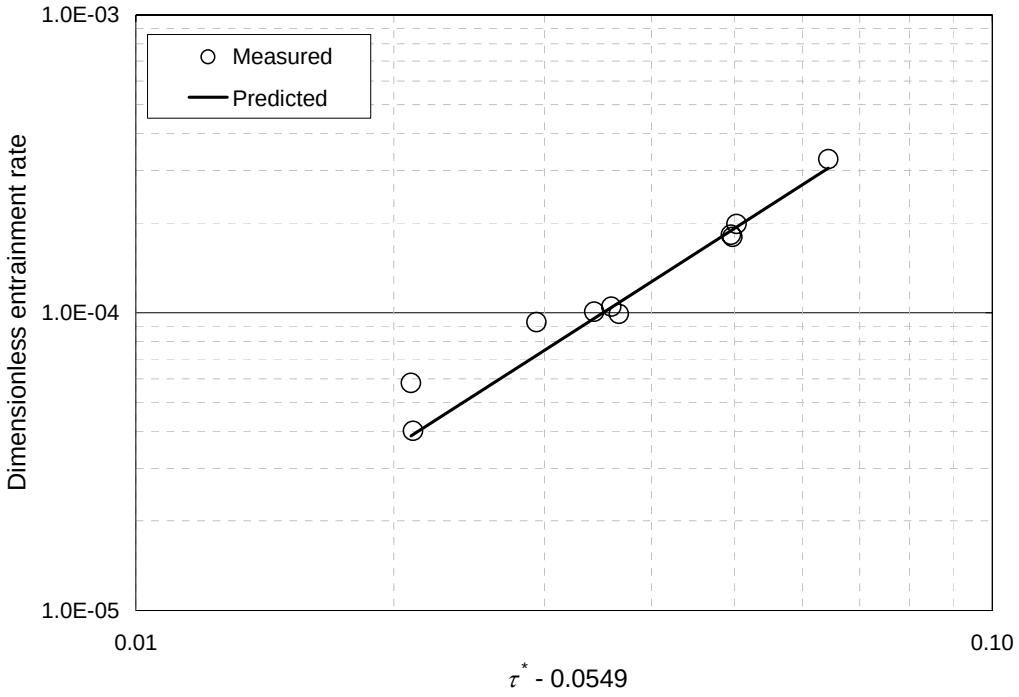
1.0E-03
1.0E-04
1.0E-05
Measured
Predicted
Dimensionless entrainment rate
0.01
0.10
τ^* - 0.0549

Figure 10

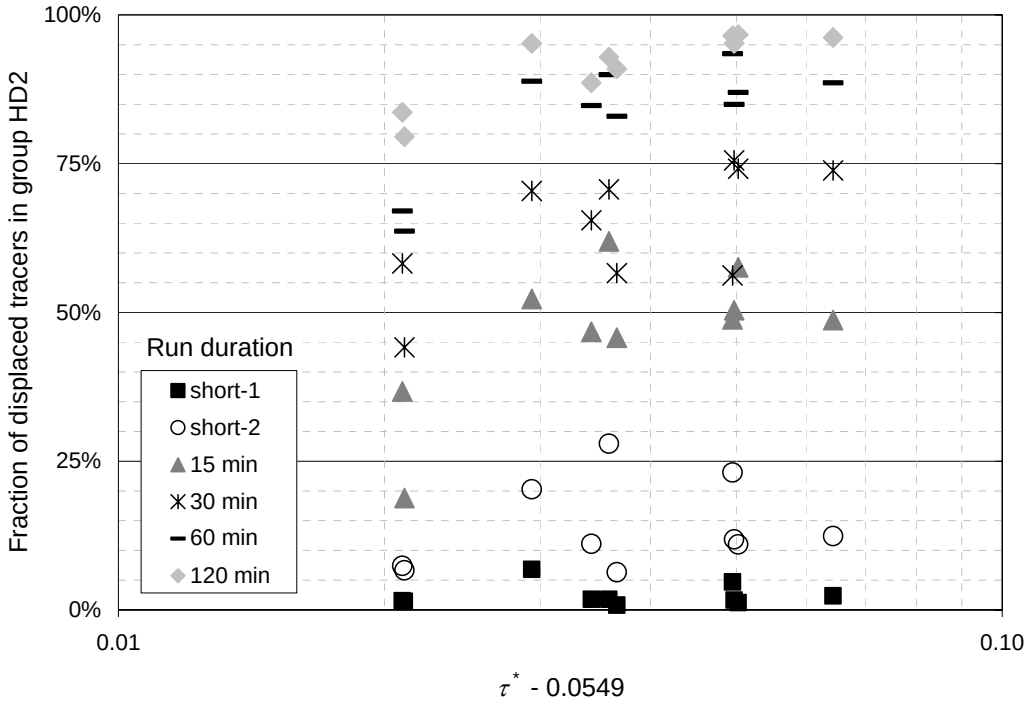
100%
75%
50%
25%
0%
Fraction of displaced tracers in group HD2
Run duration
short-1
short-2
15 min
30 min
60 min
120 min
0.01
0.10
τ* - 0.0549

Figure 11

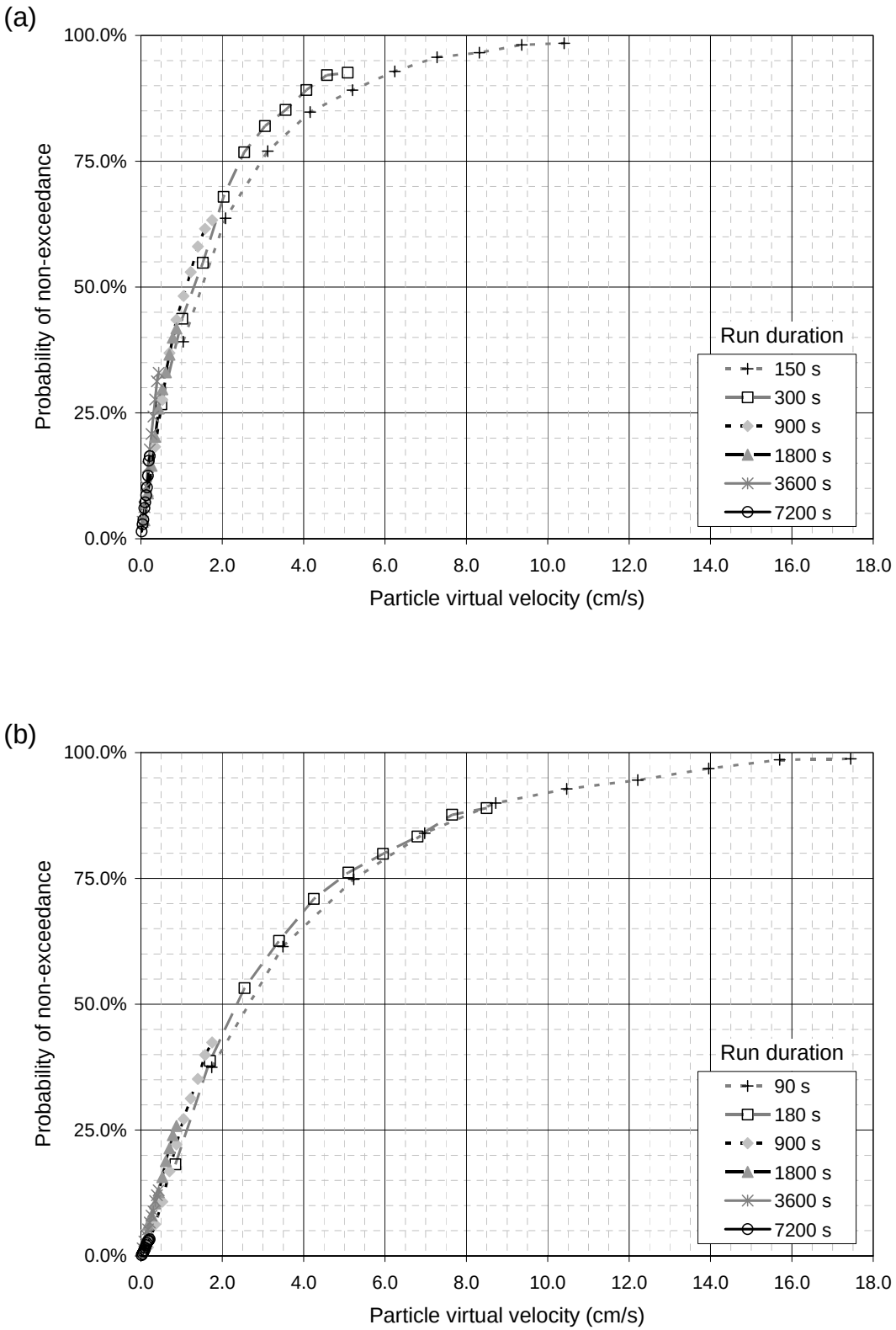
(a)
100.0%
75.0%
50.0%
25.0%
0.0%
Probability of non-exceedance
0.0
2.0
4.0
6.0
8.0
10.0
12.0
14.0
16.0
18.0
Particle virtual velocity (cm/s)
Run duration
150 s
300 s
900 s
1800 s
3600 s
7200 s
(b)
100.0%
75.0%
50.0%
25.0%
0.0%
Probability of non-exceedance
0.0
2.0
4.0
6.0
8.0
10.0
12.0
14.0
16.0
18.0
Particle virtual velocity (cm/s)
Run duration
90 s
180 s
900 s
1800 s
3600 s
7200 s

Figure 12

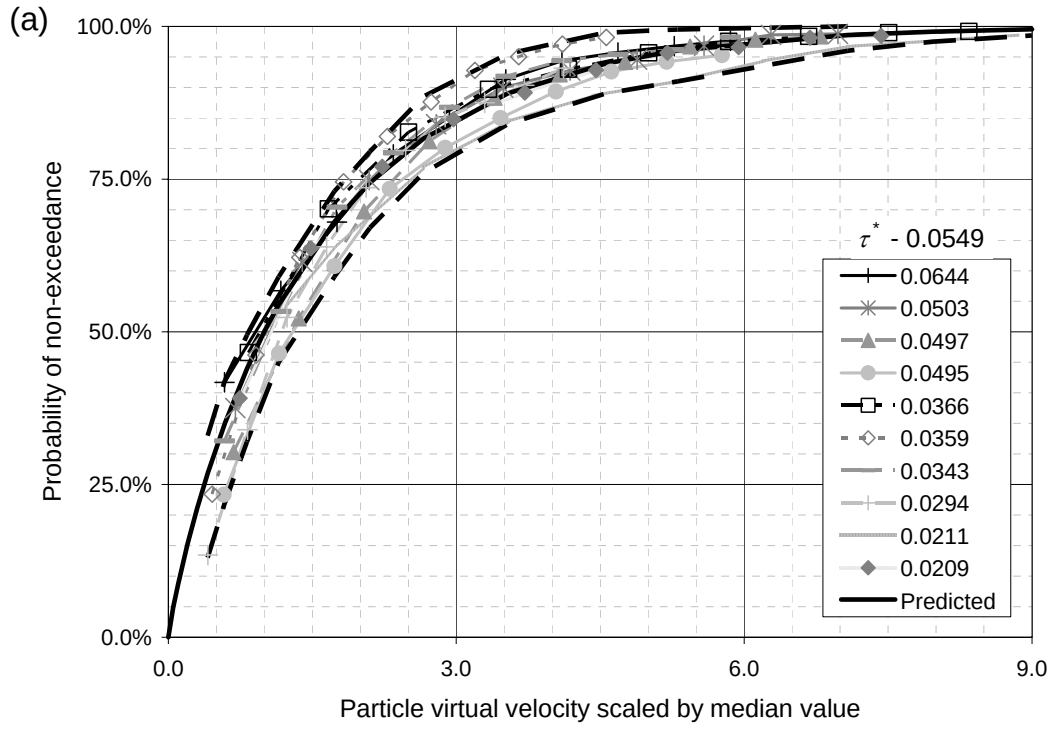
(a)
100.0%
75.0%
50.0%
25.0%
0.0%
Probability of non-exceedance
0.0
3.0
6.0
9.0
Particle virtual velocity scaled by median value
τ* - 0.0549
0.0644
0.0503
0.0497
0.0495
0.0366
0.0359
0.0343
0.0294
0.0211
0.0209
Predicted

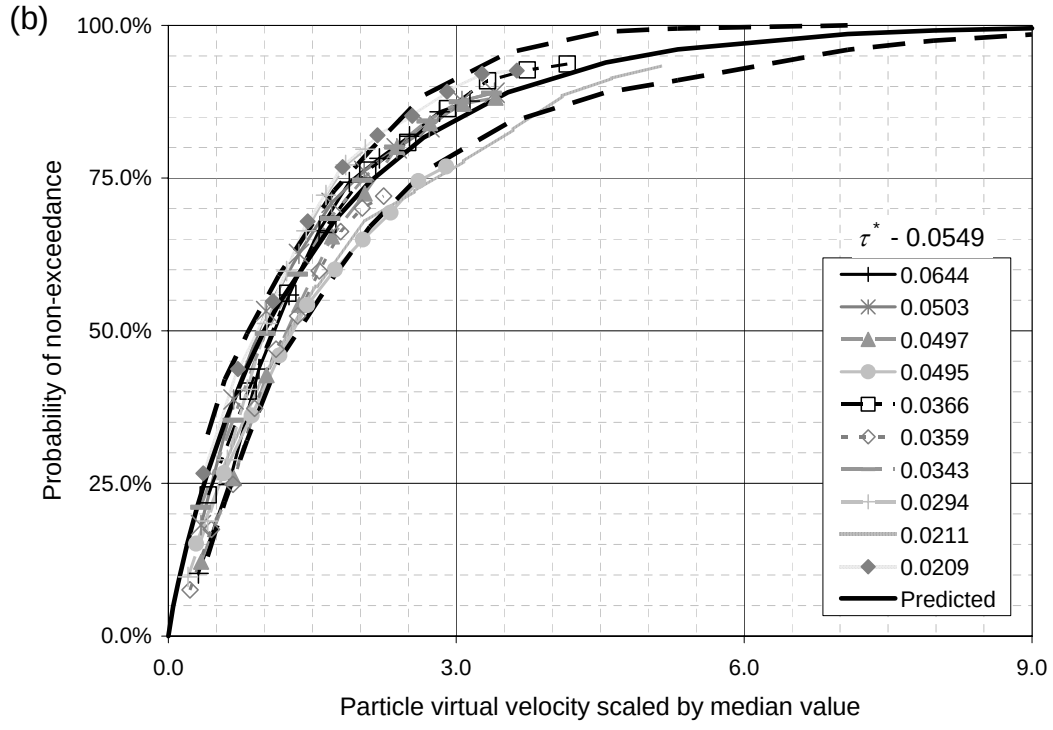
(b)
100.0%
75.0%
50.0%
25.0%
0.0%
Probability of non-exceedance
0.0
3.0
6.0
9.0
Particle virtual velocity scaled by median value
τ* - 0.0549
0.0644
0.0503
0.0497
0.0495
0.0366
0.0359
0.0343
0.0294
0.0211
0.0209
Predicted

Figure 13

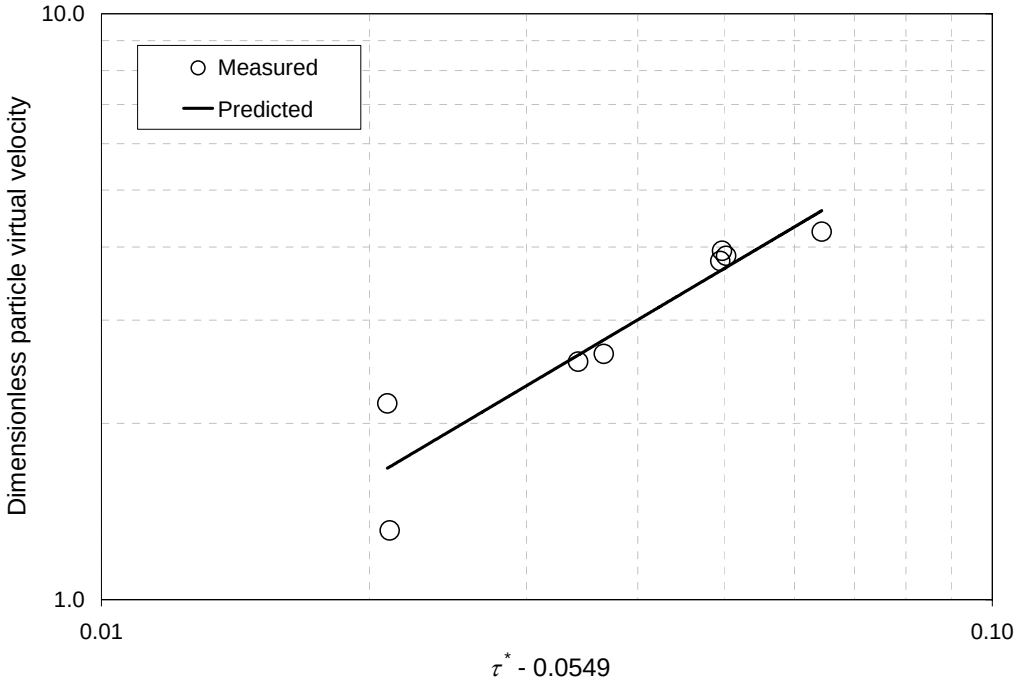
10.0
1.0
0.01
0.10
Measured
Predicted
Dimensionless particle virtual velocity
τ^* - 0.0549

Figure 14